In presenting this dissertation/thesis as a partial fulfillment of the requirements for an advanced degree from Emory University, I agree that the Library of the University shall make it available for inspection and circulation in accordance with its regulations, governing materials of this type. I agree that permission to copy from, or to publish, this thesis/dissertation may be granted by the professor under whose direction it was written, or, in his/her absence, by the Dean of the Graduate School when such copying or publication is solely for scholarly purposes and does not involve potential financial gain. It is understood that any copying from, or publication of, this thesis/dissertation which involves potential financial gain will not be allowed without written permission.

_____

Yi Xu

Exploring the peptide nanotube formation from the self-assembly of the Aβ(13-21)K16A peptide in the presence of Zinc ions

By

Yi Xu
Master of Science

Department of Chemistry

_____
Dr. David G. Lynn
Advisor

_____
Dr. Vincent P. Conticello
Committee Member

_____
Dr. Stefan Lutz
Committee Member

Accepted:

_____
Lisa A. Tedesco, Ph.D.
Dean of the Graduate School

_____
Date

Exploring the peptide nanotube formation from the self-assembly of the Aβ(13-21)K16A peptide in the presence of Zinc ions

By

Yi Xu
B.S. Nanjing University, 2001
M.S. Nanjing University, 2004

Advisor: David G. Lynn, Ph.D.

An Abstract of
A dissertation submitted to the Faculty of the Graduate School of Emory University in partial fulfillment of the requirements for the degree of
Master of Science

Department of Chemistry

2007

In vitro, Zn^{2+} accelerates the self-assembly of Aβ(13-21)K16A and induces the formation of ribbons (Dong 2006). Peptide ribbons have been proposed to be the precursors of peptide nanotubes. Theoretically, the peptide ribbons formed by Aβ(13-21)K16A can also change to peptide nanotubes. In this dissertation, temperature effects of the self-assembly of Aβ(13-21)K16A were investigated in the presence of zinc ions.

In the presence of zinc ions, Aβ(13-21)K16A peptides self assemble into ribbons at low temperatures, such as 4 ^{o}C and 24 ^{o}C. When increasing the temperature to 37 ^{o}C, these peptides self assemble into peptide nanotubes. Preformed helical ribbons can switch to peptide nanotubes with increasing temperature. Peptide nanotubes are quiet stable, and they cannot dissemble back to helical ribbons. The transaction from helical ribbons to peptide nanotubes possibly attributes to the dramatic expansion of sheet-sheet lamination.

ssNMR experiments have been tried to clarify the detail peptide arrangement in zinc induced Aβ(13-21)K16A peptide nanotubes. Cryo- and lyo- experiments show that peptide nanotubes are destroyed during lyophilization. To protect the peptide nanotubes, several anions and chelates, such as SO_4^{2-}, EDTA, terephthalic acid, hydroquinone, 1,2-ethanedithiol and 1,4-benzenedimethanethiol, have been tested to bundle the tubes. All these reagents cannot bundle the peptide nanotubes successfully.

Solvent effects on the Zn^{2+} induced Aβ(13-21)K16A peptide self-assembly have been investigated to study the physical stability of peptide nanotubes. The results show that some solvents, such as methanol and acetonitrile, can destabilize the peptide nanotubes. The higher the solvent concentration, the less stable the peptide nanotubes. Temperature effect of the peptide self-assembly at certain solvent concentrations

indicates that Zn^{2+} induced ribbons or nanotubes are more stable at lower temperature in the presence of acetonitrile.

The assembled peptide nanotubes, with such ordered and dense packed Zn^{2+} sites exposed on the surface, open the possibility to engineer temperature directed polymerization and unique catalytic chemistry.

Exploring the peptide nanotube formation from the self-assembly of the Aβ(13-21)K16A peptide in the presence of Zinc ions

By

Yi Xu
B.S. Nanjing University, 2001
M.S. Nanjing University, 2004

Advisor: David G. Lynn, Ph.D.

An Abstract of
A dissertation submitted to the Faculty of the Graduate School of Emory University in partial fulfillment of the requirements for the degree of Master of Science

Department of Chemistry

2007

ACKNOWLEDGEMENTS

First of all, I would like to thank my research advisor Professor David G. Lynn for all his support for my graduate career. As a supervisor and a mentor, he always encouraged me to find what I really need/want to do, instead of telling me what I need to do. In his lab, I began to think independently and ask "how/why" whenever I had any questions about my project. I also would thank my committee members, Dr. Vincent P. Conticello, and Dr. Stefan Lutz, supervising me over the years.

For the experiments, firstly I would like to thank Dr. Jijun Dong, my first experimental director in this lab. Dr. Jijun Dong taught me a lot of basic experiments in amyloid project, such as sample preparation, CD, FT-IR, TEM, and AFM. Also, I would like to thank Dr. Anil Mehta for his help in ssNMR experiments and computer modeling. I deeply appreciate Rong Ni for her help in every detail experiments. I also would thank Hong Yi at Department of Neurology for the use of their TEM instrument.

I am very proud of working in this large lab and having so many excellent colleagues. I would like to thank Dr. Lizhi Liang, Dr. Xiaohua Li, Dr. Rong Gao, Dr. Kun Lu, and Dr. Teresa Hill, who already left our lab, and current lab mates, Dr. Fang Fang, Dr. Anil Mehta, Dr. Trey Maddox, Dr. Melissa Bobeck, Peng Liu, Rong Ni, Yan Liang, Yi-Han Lin, Yue Liu, Seth Childers, Andrew Palmer, James Simmons, Kornelius Bankston. I also would like to thank all my friends in Emory.

Most of all, I really want to thank my father Zhengmin Xu, my mother Zhilan Zhang and my girl friend Weilin Peng for their love, support and encouragement over the years.

TABLE OF CONTENTS

LIST OF FIGURES

LIST OF TABLES

LIST OF ABBREVIATIONS

Å	Angstrom
aa	amino acids*
Aβ	Amyloid β peptide
AD	Alzheimer's Disease
AFM	Atomic Force Microscopy
CD	Circular Dichroism
Cryo-etch HRSEM	Cryo-etch High Resolution Scanning Electron Microscopy
EXAFS	Extended X-ray Absorption Fine-Structure
Fmoc	FlourenylMethOxyCarbonyl
FT-IR	Fourier Transform Infrared Raman spectroscopy
HPLC	High-Performance Liquid Chromatograph
Hz	Hertz
MES	2-Morpholino Ethane Sulfonic acid
MeCN	Acetonitrile
min	minute
ml	mili-liter
mM	milli-Molar
μM	micro-Molar
MRME	Molar Residue Mean Ellipticity
NMM	4-methylmorpholine
NMR	Nuclear Magnetic Resonance
ss-NMR	solid state NMR

TEM	transmission electron microscopy
TFA	trifluoroacid
UV	ultra-violet

* All amino acids were abbreviated according to the standard three-letter or one-letter codes.

CHAPTER 1

INTRODUCTION

Protein based nanobiomaterials

Nanomaterials are the theme of the contemporary era because of their unique functional properties in optics, mechanics, electronics and magnetics (Sarikaya 2004). Self-assembly plays an important role in constructing and processing nanomaterials (Zhang 2002). Molecular self-assembly is characterized by spontaneous diffusion and specific association of molecules dictated by non-covalent interactions, such as van der waals bonds, electrostatic interactions, hydrogen bonds and stacking interactions. During the past decade, many examples of biomolecules, including DNA (Seeman 2002), peptides (Zhang 2003; Dong 2002; Lu 2003; Rapaport 2000), and proteins (Ringler 2003; Sleytr 2003), have been used to form well-defined structures with specific functionalities by self-assembly.

Various properties endowed by the biocompatibility of the 20 different amino acids have enabled proteins to function as building blocks for creation of novel biomaterials. On the other hand, the development of biotechnology and genetic engineering, together with peptide synthesis techniques, facilitate the advances in protein

based nanomaterials.

In protein based nanomaterials, self-assembled peptide nanotubes gain more and more attention. Since the discovery of carbon nanotubes (CNT) by Sumio Iijima in 1991 (Iijima 2001), such nanosized hollow tubular structures have generated exceptional interest in diverse chemical, biological, electrical and mechanical based material science settings. However, the inabilities to solubilize and separate individual carbon nanotubes in water present a great challenge for applications in biological system. In contrast, peptide nanotubes can provide a solution to overcome these difficulties encountered by CNT in biological systems. First, peptide nanotubes can function as molecular scaffolding and container devices. Second, peptide nanotubes have good biocompatibility and higher solubility. Finally, peptide nanotubes can be easily modified by other groups. Several other peptide nanotubes have been constructed (Valèry 2003; Ghadiri 1993). Both of the peptides in these two peptide nanotubes contain *D*-amino acids. In our lab, we have constructed homogenous peptide nanotubes by *L*-amino acids (Lu 2003). The peptide sequence in this peptide nanotube is KLVFFAE, also called Aβ(16-22), a short fragment from amyloid β peptide.

Amyloid β peptide

Alzheimer's disease is an irreversible progressive brain disorder, which can destroy not only a person's learning, judgment and communication skills but also the ability to carry out daily activity. One of the most significant characteristics of Alzheimer's disease is the accumulation of amyloid plaques between nerve cells in the brain. The amyloid plaques are mainly composed of aggregates of amyloid β peptide. Aβ

peptide is a 38 to 43 amino acid proteolytic fragment derived by proteoytic cleavage of amyloid precursor protein (Hardy 2002). Aβ peptides show the alternating hydrophilic and hydrophobic patterns, including a hydrophilic N-terminus (residues 1-16), a central hydrophobic region (residues 17-21), a small central hydrophilic region (residues 22-28), and a long and very hydrophobic C-terminus (residues 29-42) (Figure 1.1). Particularly, Aβ(1-40) is the predominant soluble peptides consisting ~ 90 % of all Aβ peptide, but it appears to be minor component in amyloid plaques; and Aβ(1-42) is the major component of the amyloid plaque (Gowing 1994).

^{1}DAEFRHDSG^{10}YEVHHQK**LVF^{20}FA**EDVGSNK**G^{30}AIIGLMVGGV^{40}VIA**

Figure 1.1. The sequence of Aβ(1-42). Red and blue sequences mean hydrophilic and hydrophobic regions, respectively.

Because of the large molecule weight, insolubility and non-crystallinity of aggregation of amyloid peptides, it is difficult to obtain high-resolution structural characterization of amyloid fibrils by solution NMR and X-ray crystallography. However, the structure of amyloid fibrils has been obtained by low-resolution techniques, such as X-ray diffraction, FT-IR, circular dichroism as well as solid-state NMR. Previous X-ray diffraction studies suggest that amyloid fibrils are composed of numerous β-strands, which associate into β-sheet with hydrogen bonds parallel to the long axis of the fibril, while β-sheets laminate perpendicular to the fibril axis (Kirschner 1986). The distance between the adjacent β strands is 5 Å, and the distance between the adjacent laminates is

10 Å (Kirschner 1986). In our lab, solid state NMR has been used to measure the backbone carboxyl-carboxyl and/or carboxyl-amide distances of amyloid fibrils formed by Aβ(10-35) (Burkoth 2000; Benzinger 2000). The distances measurement suggests a parallel in-register β strand alignment (Figure 1.2). Further investigation on amyloid fibrils were performed on several truncated and/or mutated Aβ peptides, such as Aβ(10-21) (Morgan 2002), Aβ(13-21)K16A (Dong 2006) and Aβ(16-22) (Lu 2003).

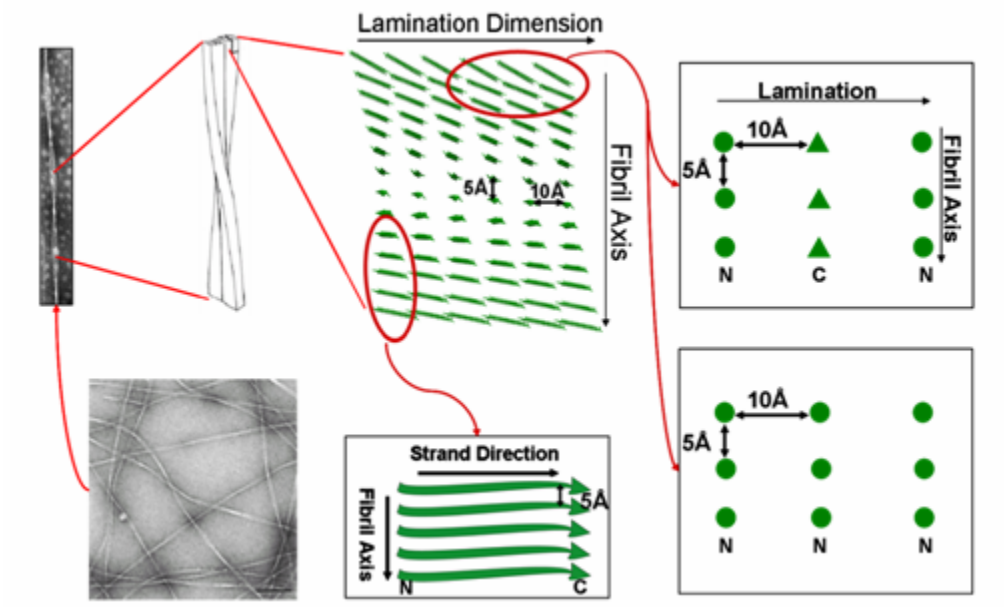

Figure 1.2. Structural model proposed for Aβ(10-35). Single green line, one Aβ(10-35) molecule; arrow, C-terminus of the peptide.

Zinc effect in amyloid formation

Metal ions, such as Zn^{2+}, Cu^{2+} and Fe^{3+}, play important roles in amyloid aggregation, neurotoxicity and Alzheimer's disease. For example, abnormal concentration of Zn^{2+} has been shown to be present in the amyloid plaques in Alzheimer's disease brain (Assaf 1984). Zn^{2+} triggers the rapid and extensive aggregation

of Aβ peptide in canine cerebrospinal fluid (Bush 1994). Trace amounts of copper induce the formation of amyloid plaque and learning deficits in a rabbit model of Alzheimer's disease (Sparks 2003). Also, the treatment of Alzheimer's disease can be achieved by antibiotic clioquinol, a known Cu^{2+}/Zn^{2+} chelator (Cherny 2001).

Mutagenesis and pH dependence studies on human Aβ peptide self-assembly in the presence of Zn^{2+} show that His13 is crucial for the Zn^{2+} binding (Liu 1999; Curtain 2001). Based on the structures of the different amyloid fibrils, there are two kinds of possible Zn^{2+} coordination environments (Morgan 2002) (Figure 1.3). The first potential binding site is between two β strands within a single sheet, and the second potential binding site is between two β strands of adjacent β sheets.

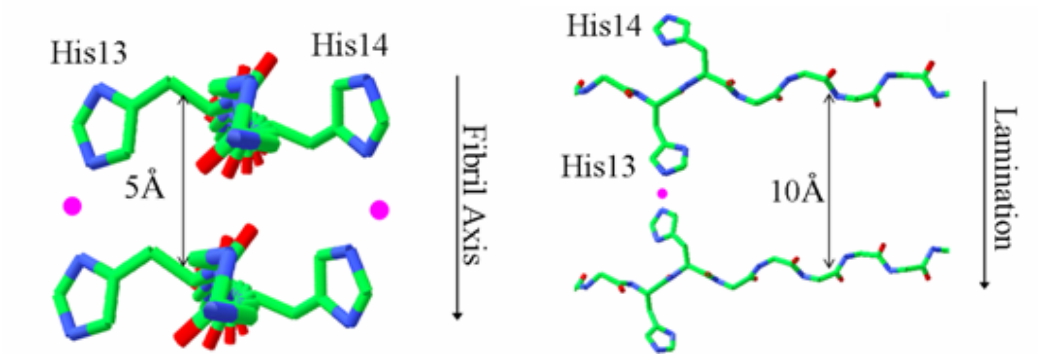

Figure 1.3. Left: potential binding sites between two strands within a sheet. Right: potential binding sites between two strands of different sheets. Pink dots represent zinc ions.

To simplify the Zn^{2+} binding models of Aβ peptide, several truncated Aβ peptides, such as Aβ(10-21) and Aβ(13-21)K16A, have been investigated in our lab (Morgan 2002; Dong 2006). Studies on Aβ(10-21) show that Zn^{2+} will facilitate the self-assembly of Aβ(10-21) to induce amyloid fibril formation. Studies on the mutant Aβ(10-21)H13Q

have been used to identify the most possible Zn^{2+} binding model. Based on the left model in Figure 1.3, it is also possible for Zn^{2+} to accelerate the self-assembly of Aβ(10-21)H13Q by binding between two His14. On the other hand, studies on the mutant Aβ(10-21)H13Q show that the self-assembly of mutant peptide is independent of Zn^{2+}. Therefore, it can be proposed that Zn^{2+} coordinates to His13 and His14 from adjacent laminates (Morgan 2002).

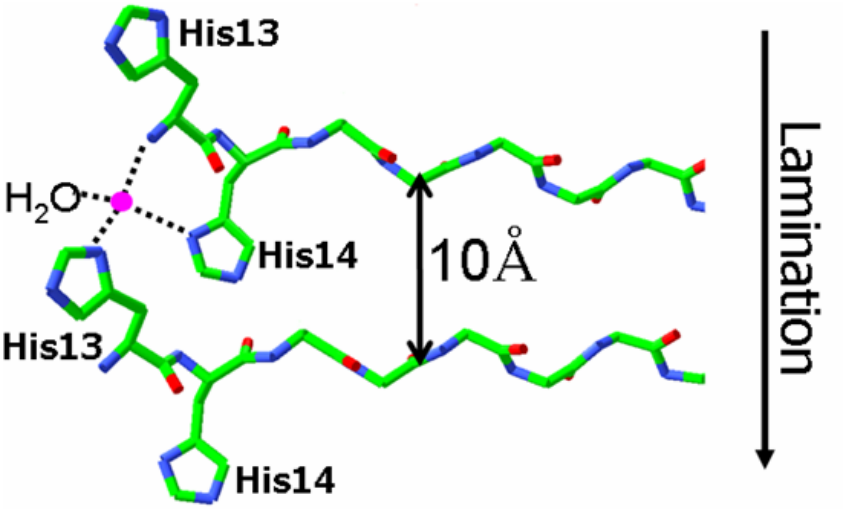

Figure 1.4. Proposed model for the Zn^{2+} coordination environment between two adjacent sheets along the lamination dimension. Pink dot represents zinc ion.

For Aβ(13-21)K16A, isotope edited FT-IR and solid state NMR studies show that Zn^{2+}-induced ribbon structures have an anti-parallel β sheet structure. In this situation, Zn^{2+} cannot coordinate to His13 and His14 from adjacent β strand within the single β sheet. Therefore, the most likely place where Zn^{2+} can coordinate to histidine residues is between His13 and His14 from the adjacent laminates. As a result, at high Zn^{2+} concentration, Zn^{2+} is proposed to be coordinated between adjacent β sheets and therefore stabilizes the β sheet lamination and increases the growth of lamination (Dong 2006)

(Figure 1.4). Based on this model, Zn^{2+} is coordinated to two histidine residues, an N terminal amino group, as well as a water molecule. Because the N terminus of the Aβ(13-21)K16A is exposed to the surface of the Zn^{2+}-induced ribbon structures, zinc ions are incorporated one by one on the surface of the ribbon, with the 10 Å distance in both hydrogen bonding direction and lamination direction..

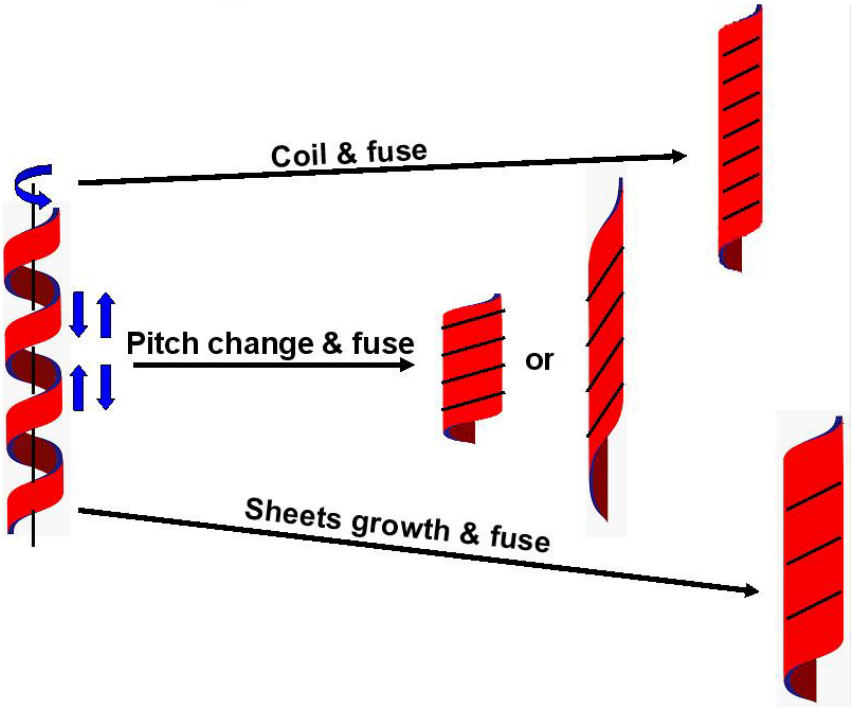

Figure 1.5. Possible pathways from ribbons to tubes.

It has been widely proposed that peptide ribbons are the precursors of peptide nanotubes. Usually, the rectangular sheet twists to form helical peptide ribbons, and the ends of the ribbons will meet together and fuse to form peptide nanotubes (Lu 2003). For Aβ(13-21)K16A peptide, in the presence of Zn^{2+}, peptides can self assemble into twisted peptide ribbons at room temperature. So, how can these twisted ribbons become peptide nanotubes? As is shown in Figure 1.5, there're three different pathways form ribbons to

nanotubes. At first, ribbons can change to nanotubes by coiling and fusing. Under this condition, the pitch of peptide arrangement does not change. Secondly, by pitch change and fusing, ribbons can also switch to nanotubes. Finally, by sheets growth and fusing, ribbons can change to nanotubes. Under this condition, the pitch of peptide arrangement does not change, and the beta sheet population in whole system increases with the sheets growth.

In this thesis, further studies have been applied to the self-assembly of the nine-residue peptide cassette from Aβ peptide, Aβ(13-21)K16A. It has been widely acknowledged that outside stimuli, such as pH, temperature, and ionic strength, can control the protein folding and peptide self-assembly by changing the driving force. In the presence of Zn^{2+}, the studies of temperature effect indicate that peptide nanotubes are self assembled by increasing the system temperature from room temperature to 37 ^{o}C. A possible explanation is that at lower temperature range, increasing temperature results in the increase of hydrophobic interaction.

CHAPTER 2

EXPLORING THE PEPTIDE NANOTUBE FORMATION FROM SELF-ASSEMBLY OF THE Aβ(13-21)K16A PEPTIDE IN THE PRESENCE OF ZINC IONS

INTRODUCTION

Previous studies in our lab show that in the presence of Zn^{2+}, Aβ(13-21)K16A peptides will self assemble into twisted ribbons with widths of 100-200 nm after one month incubation at room temperature (Dong 2006). Peptide ribbons have been proposed to be the precursors of peptide nanotubes. The edges of this rectangular sheet, which twist to form helical peptide ribbons, meet together and fuse to form peptide nanotubes. Theoretically, the peptide ribbons formed by Aβ(13-21)K16A can also change to peptide nanotubes. We propose that several outside stimuli can control the transaction between the peptide ribbons and peptide nanotubes by changing the driving forces of peptide self-assembly. It has been demonstrated that some stimuli, such as temperature, pH, and ionic strength, will cause some changes in protein folding and peptide self-assembly (Schneider 2002; Pochan 2003; Ozbas 2004).

Specifically, temperature plays important roles on protein folding and peptide self-assembly by changing the hydrophobic interaction and hydrogen bonding (Urry 1993). A typical example of the temperature effect on protein folding is the inverse temperature transition (ITT) behavior of elastin (Urry 2002). At lower temperature, elastin exists in the form of a random coil. With increasing temperature, elastin undergoes hydrophobic collapse above its transition temperature, expelling waters formerly associated with non-polar residues. A lot of work has been done to study the interaction between temperature and hydrophobic interaction. Hydrocarbons are typical of hydrophobes. Usually, their solubility decreases with increasing temperature at low temperatures, which provides an important clue to the mechanism of hydrophobicity. At higher temperatures, the solubility, after reaching a minimum, often then increases with further increase of temperature (Widom 2003). Similar results can also be found in protein folding. For example, the free energy of myoglobin folding increases with the increasing temperature at first, and then decreases slowly (Southall 2002). These changes also suggest that at lower temperature, hydrophobic interaction will increase intensity with increasing temperature. In our lab, Seth Childers found that varying the temperature will change the final morphology of the self-assembly of Aβ(16-22). Here, I also want to study the temperature effect on the self-assembly of Aβ(13-21)K16A peptide in the presence of zinc ions.

MATERIALS AND METHODS

Materials

Fmoc-amino acids, resins and solid phase peptide synthesizer reagents were

purchased from Novabiochem (San Diego, CA). Distilled deionized water for sample preparation was obtained from EMD chemicals Inc. (Gibbstown, NJ). DMF, HPLC grade acetonitrile and methanol, and $Zn(NO_3)_2$ (99.999 %), 2-morpholinoethanesulfonic acid monohydrate (MES, ≥ 99.5 %) and all other reagents were obtained from Aldrich Chemical Co. (Milwaukee, WI).

Synthesis and purification of Aβ(13-21)K16A: HHQALVFFA-NH_2

Aβ(13-21)K16A, HHQALVFFA-NH_2, was synthesized on a Rainin Symphony Quartet multiplex solid-phase peptide synthesizer using standard FMOC chemistry on FMOC Rink-amide polystyrene resin (Novabiochem, Inc., usually with substitution 0.4-0.6 meq/g) and HBTU/NMM as the coupling reagents. His14, Gln15 and Ala16 were double coupled to give a high couple yield. A capping step with acetylation was included after each coupling reaction to prevent the formation of deletion peptides. The peptide was cleaved and deprotected using a mixture of 90 % trifluoroacetic acid, 5 % thioanisole, 3 % ethanedithiol, and 2 % anisole for two hours at room temperature, at a ratio of 10 mL per 100 meq. The crude peptides were precipitated and washed 4-5 times with chilled anhydrous ethyl ether and dried under vacuum. The peptide was then purified using a Waters Delta 600 HPLC with Waters Atlantis C-18 preparative HPLC column (19 x 250 mm) and eluted at 10 mL/min with a linear gradient from H_2O/MeCN (8:2) with 0.1 % TFA to H_2O/MeCN (6:4) with 0.1 % TFA over 40 min. With this gradient, Aβ(16-22) was eluted at ~ 20 min with the detection wavelength at 222 nm. The peptide fractions were collected, rotary evaporated to remove MeCN/TFA, then frozen and lyophilized. Lyophilized peptide was stored at 4 °C until required.

For synthesis of isotopic labeled peptides, isotope-labeled amino acids (Cambridge isotope laboratories, Andover MA) were Fmoc protected before peptide synthesis (Carpino et al. 1972) and the protected amino acids manually loaded during the synthesis. The synthesis and purification protocols are identical with the non-labeled peptides.

Sample preparation

The peptide powder was dissolved completely in distilled de-ionized H_2O with sonication for 10 min and centrifugation at 16,110xg for 10 min to remove preformed aggregates, if any. The supernatant was used as the peptide stock solution. The supernatant peptide stock was dilute to desired solution conditions with the following stock solution: 50 mM MES buffer at pH 5.6 and 100 mM $Zn(NO_3)_2$. Normally, the final peptide concentration is 0.5 mM in the presence of 25 mM MES buffer at pH 5.6 and the indicated Zn^{2+} concentration.

Circular Dichroism Spectroscopy (CD)

CD spectra were recorded at JASCO-810 CD spectropolarimeter at room temperature. Typically, spectra between 260 nm and 190 nm were collected with a 0.1 mm path length quartz cuvette, with a step size of 0.2 nm and a speed of 50 nm/s. Three spectra were recorded for each sample and averaged automatically. The ellipticity (θ) with unit mdeg was converted to mean residue molar ellipticity (MRE, [θ], $deg \cdot cm^2 \cdot dmol^{-1}$) by $[\theta]=\theta/(10\times n\times C\times l)$, where n is the number of amide bonds per peptide, C is the molar concentration (mol/L) and l is the cell path in cm.

Transmission Electron Microscopy (TEM)

Aliquots (10 μl) of an incubated Aβ(13-21)K16A solution were placed on Formvar/Carbon-coated 200 mesh copper grid (Electron Microscopy Science, Hatfield, PA) and allowed to settle for one minute, and the excess solution was wicked away with filter paper. The grid was placed on the upper surface of a drop of 1.5 % phosphotungstic acid or uranyl acetate solution for 2 minutes and the excess staining solution was wicked away. All samples were stored in a desiccator before study. The micrographs were obtained on a Hitachi H -7500 transmission electron microscope instrument with a LaB6 emission filament at an accelerating voltage of 75 kV at Neurology Microscopy Core Laboratory. Negatives were scanned at 600 dpi resolution on an Agfa DuoScan flatbed scanner (Agfa Corp., Ridgefield park, NJ).

FT-IR spectroscopy

FT-IR experiments were performed on wild type Aβ(13-21)K16A. After maturation, Na_2SO_4 stock solution at 725 mM was added to the sample solution to obtain final Na_2SO_4 concentration of 20 mM. White precipitates were gradually induced by Na_2SO_4. The precipitate was spun down at 16,100xg for 10 min and the pellet was frozen and lyophilized.

The dry samples were mixed with KBr at a ratio between 1:5 and 1:10 (w/w), ground into fine powder, and pressed into transparent KBr disk. FT-IR spectra were collected on Nicolet Magna 560 IR spectrometer. Typically, spectra were collected with 4 cm^{-1} resolution. One hundred scans were recorded for each sample and averaged

automatically.

Small Angle X-ray Scattering (SAXS)

SAXS experiments were carried out at room temperature on the BESSRC-CAT beam-line of Argonne National Laboratory's Advanced Photon Source (APS). Data were collected using a 15 cm × 15 cm, high-resolution, position-sensitive, nine element-tiled, CCD mosaic detector and exposure time was approximately 0.5 seconds for each measurement. Typically, five successive measurements were recorded for each sample and then averaged to obtain a final scattering profile. Sample to detector distance was ~2 m and energy of X-ray radiation was set to 12 keV. A Biologic SFM 400 stopped-flow apparatus with a 1.0 mm diameter cylindrical quartz capillary of 0.01–0.02 mm wall thickness was mounted at the beam-line. About 100 μL peptide solution was delivered into the quartz capillary and exposed to the X-ray beam. Samples were measured under constant gas flow conditions to reduce potential radiation damage. There was no evidence that samples changed over the time interval of exposure. The measurement of each sample was preceded by a measurement of the same buffer solution used in protein sample preparation. The buffer measurements provided a check on beam properties and the cleanliness of the sample cell between sample measurements as well as the means for background subtraction.

The SAXS data were reduced following routine procedures at BESRRC and the analysis of the data were carried out using the macros developed on Igor Pro platform at the Intense Pulsed Neutron Source, Argonne National Laboratory. The reduced data were averaged over the 10 measurements for further analysis in Igor Pro. Small angle

scattering intensity, $I(Q)$, can be described by

$$I(Q) = I_0 n(\Delta\rho)^2 V^2 P(Q) + I_b$$

for a dilute system of scattering particles where I_0 is an instrument constant, n is the number density of particles, $\Delta\rho$ is the difference in scattering length density (contrast) between particles and solvent, V is the volume of particles, I_b is the flat background intensity, and $P(Q)$ is the particle form factor. Q is the momentum transfer given by $Q = (4\pi/\lambda)\ sin\ (\theta/2)$ where λ is the neutron or x-ray wavelength and θ is the scattering angle. Several models were investigated, but only P(Q) for hollow cylindrical particles accurately fit the data.

$$P(Q) = \int_0^1 \left(\frac{1}{1 - \left(R_2 / R_1 \right)^2} \right)^2 \left[\frac{2J_1\left(QR_1 \left(1 - x^2\right)^{0.5} \right)}{QR_1 \left(1 - x^2\right)^{0.5}} - \frac{\left(R_2 / R_1 \right)^2 2J_1\left(QR_2 \left(1 - x^2\right)^{0.5} \right)}{QR_2 \left(1 - x^2\right)^{0.5}} \right]^2 \left(\frac{Sin\left(QHx/2 \right)}{QHx/2} \right)^2 dx$$

---Eq. 2-2

Here R_1 is the outer radius, R_2 the inner radius; H the height of the cylinder and $J_1(x)$ is the Bessel function of the first order.

RESULTS

Temperature changes Zn^{2+}-induced Aβ(13-21)K16Aself-assembly

As is shown in Figure 2.1a, in the presence of Zn^{2+}, the self-assembly of Aβ(13-21)K16A at pH 5.6 has been tested by circular dichroism (CD) at three different temperatures, 4 ^{o}C, 24 ^{o}C, and 37 ^{o}C. At higher temperature, the self-assembly of Aβ(13-21)K16A results in increased β sheet structure, showing an increase in mean residue

molar ellipticity (MRE) at 199 nm and 224 nm. The negative minima at 224 nm are plotted as a function of time for the first two weeks (Figure 2.1b). The results show that at 37 ^{o}C, the peptide solution contains increased β sheet structure over those at 4 ^{o}C and 24 ^{o}C. At 37 ^{o}C, the development of β sheet structure is confirmed by FT-IR with the appearance of the amide carbonyl structure at 1632 cm^{-1}, which is similar to the FT-IR spectrum of this peptide at room temperature (Dong 2006) (Figure 2.1c).

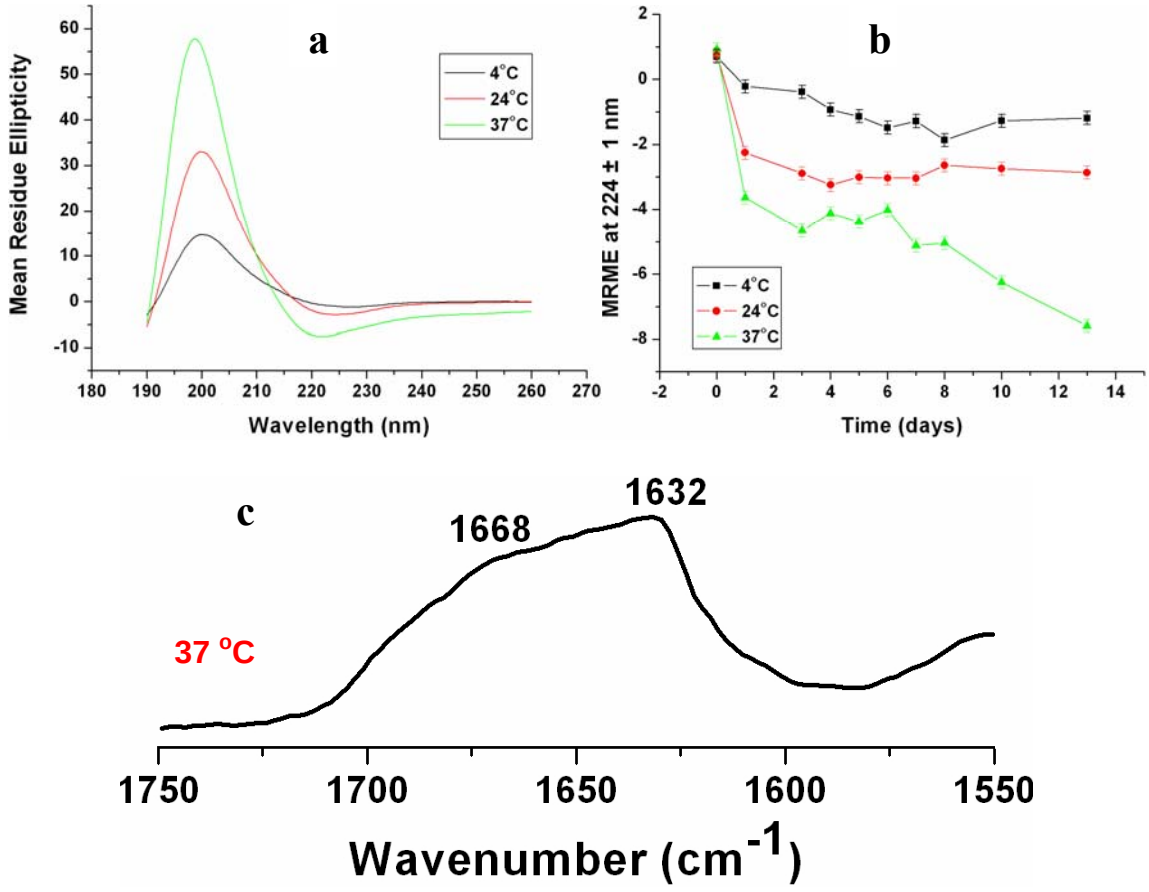

Figure 2.1. Temperature-dependent CD spectra of 0.5 mM Aβ(13-21)K16A in 25 mM MES buffer at pH 5.6 in the presence of 0.5 mM Zn^{2+}. (a) CD spectra collected after 30 days incubation; (b) The plot of CD intensity at around 224 nm for the first two weeks. (c) FT-IR spectra of Aβ(13-21)K16A at 37 ^{o}C.

TEM images revealed that Aβ(13-21)K16A self-assembles into different morphologies at different temperatures (Figure 2.2, 2.3). Figure 2.2 shows the images after three days' incubation. At 4 ^{o}C and 24 ^{o}C, peptides self assembled into ribbons, with the average width 41nm and 70nm, respectively. At 37 ^{o}C, peptides self assembled into the mixture of helical ribbons and peptide nanotubes. The average width of ribbons is 148 nm. Figure 2.3 shows the TEM images taken after four weeks' incubation. At 4 ^{o}C, most peptides self assembled in to helical ribbons, and there is a small portion of nanotubes. The average width of ribbons is 157 nm. At 24 ^{o}C, the percentage of tubes increases, but there is still a large portion of ribbons. The average width of ribbons is 243 nm. When the peptides were incubated at 37 ^{o}C, almost all peptides self assembled into peptide nanotubes, with a width between 150 nm to 350 nm. The average width is 247 nm. Clearly, increasing temperature can increase the sheets lamination during the self-assembly process. As a result, the most probable model from ribbons to nanotubes is sheets increasing and fusing.

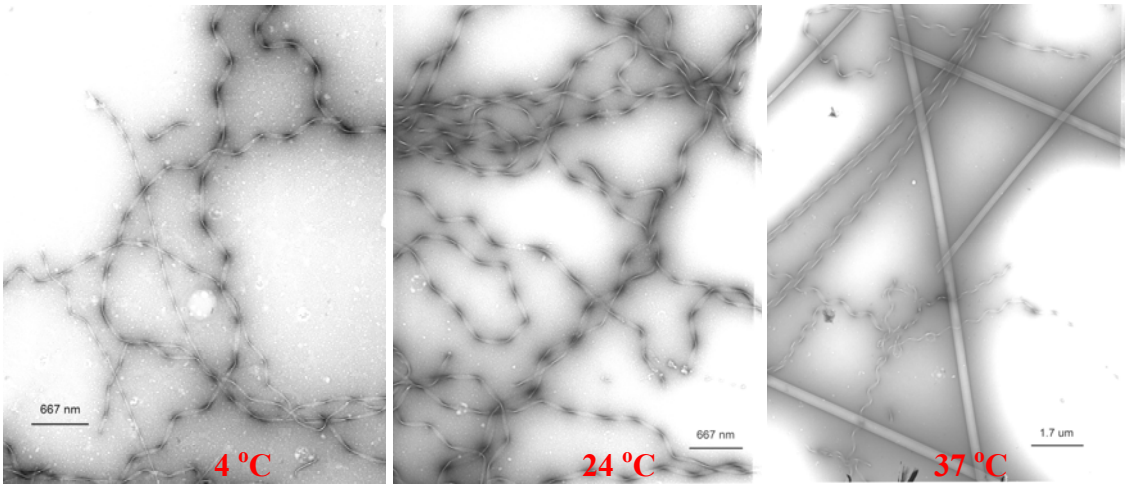

Figure 2.2. Temperature-dependent TEM images of 0.5 mM Aβ(13-21)K16A in 25 mM MES buffer at pH 5.6 in the presence of 0.5 mM Zn^{2+} after three days at the indicated

temperatures.

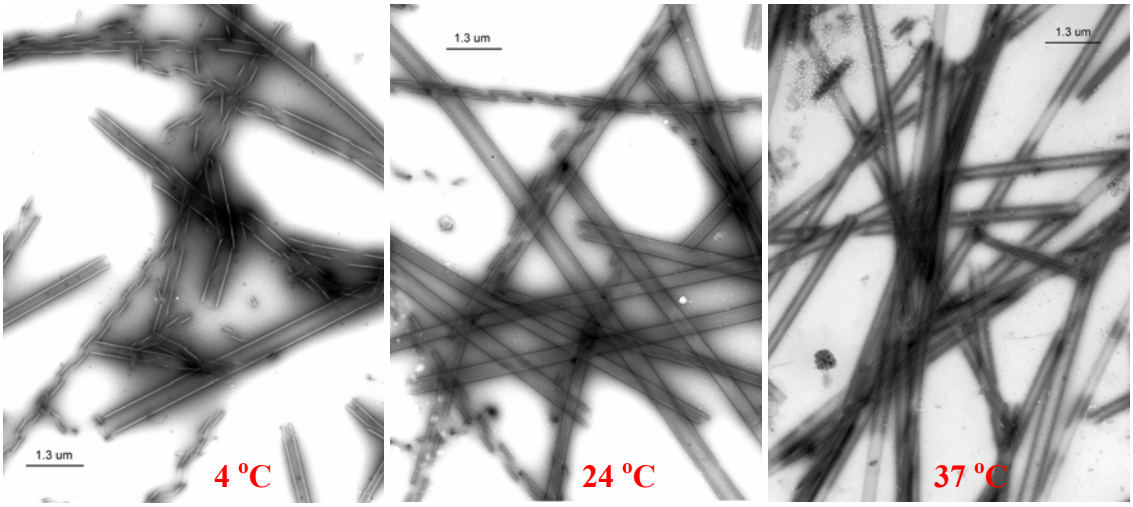

Figure 2.3. Temperature-dependent TEM images of 0.5 mM Aβ(13-21)K16A in 25 mM MES buffer at pH 5.6 in the presence of 0.5 mM Zn^{2+} after four weeks at the indicated temperatures.

The above data show that peptides can self assemble into different morphologies when peptides are incubated at different temperatures. Next, stability studies were processed for the ribbons and nanotubes. As is shown in Figure 2.4, the preformed peptide ribbons, which were incubated at 4 ^{o}C, were divided into three and incubated at three different temperatures. The CD intensity at around 224 nm increased dramatically with increasing temperature. TEM images were also consistent with the CD intensity. When comparing the images taken after four weeks with those taken after two weeks, we can find that the ribbons switch to tubes at elevated temperature. Figure 2.5 shows the CD and TEM results of the peptides, which were incubated at 37 ^{o}C at the first two weeks and then divided into three and incubated at lower temperatures. The CD intensity at

around 224 nm shows no big changes. Also, TEM images are consistent with the CD intensity, and no big difference is appearing from the TEM images. As a result, ribbons can switch to peptide nanotubes with increasing temperature. On the other hand, zinc-induced peptide nanotubes are thermostable, and they will not break down and switch to ribbons at lower temperature (Figure 2.6a). As shown in Figure 2.6b, I propose that peptide ribbons are higher in free energy than peptide nanotubes. The transaction from ribbons to tubes can be introduced but not the reverse. As a result, ribbons can switch to tubes easily, and tubes can not dissemble back to ribbons.

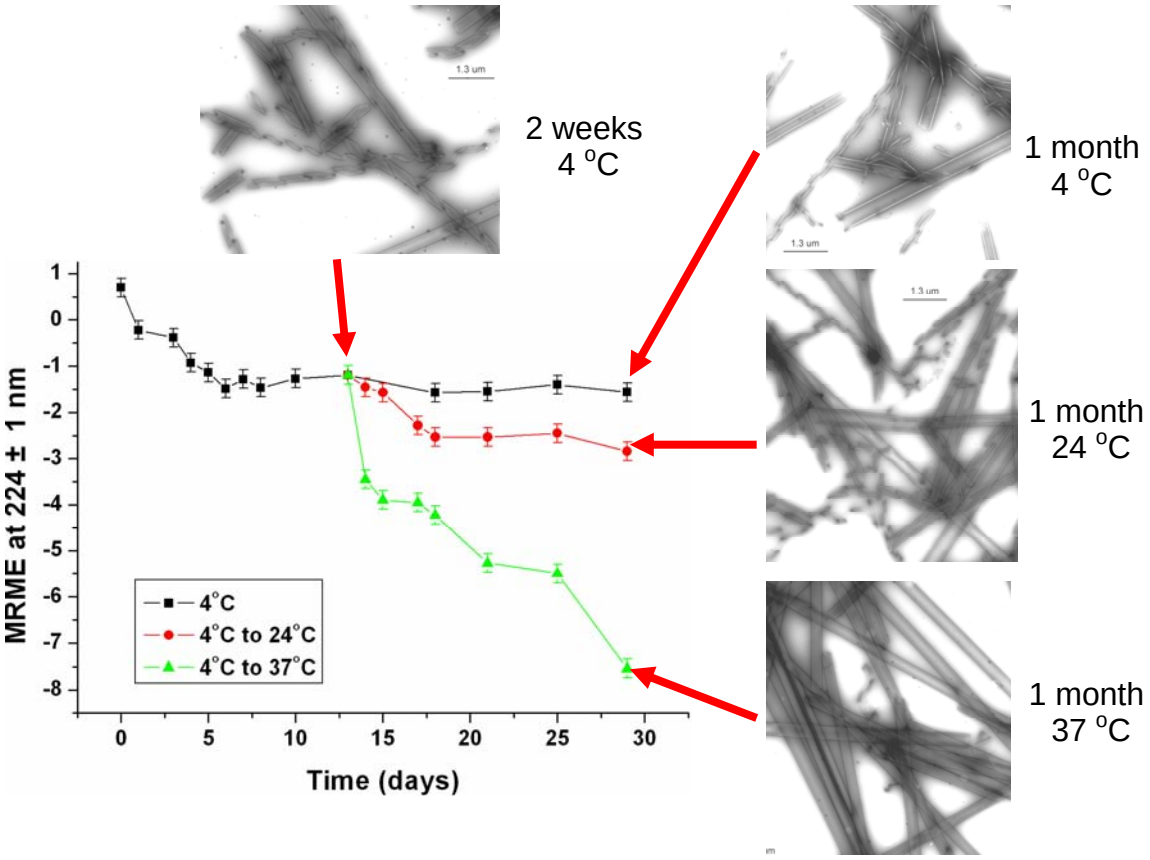

Figure 2.4. The plot of CD intensity at 224 nm for the first four weeks. After incubating at 4 °C for two weeks, sample was divided into three and incubated at three different temperatures, respectively. TEM images were taken after two weeks and after four weeks.

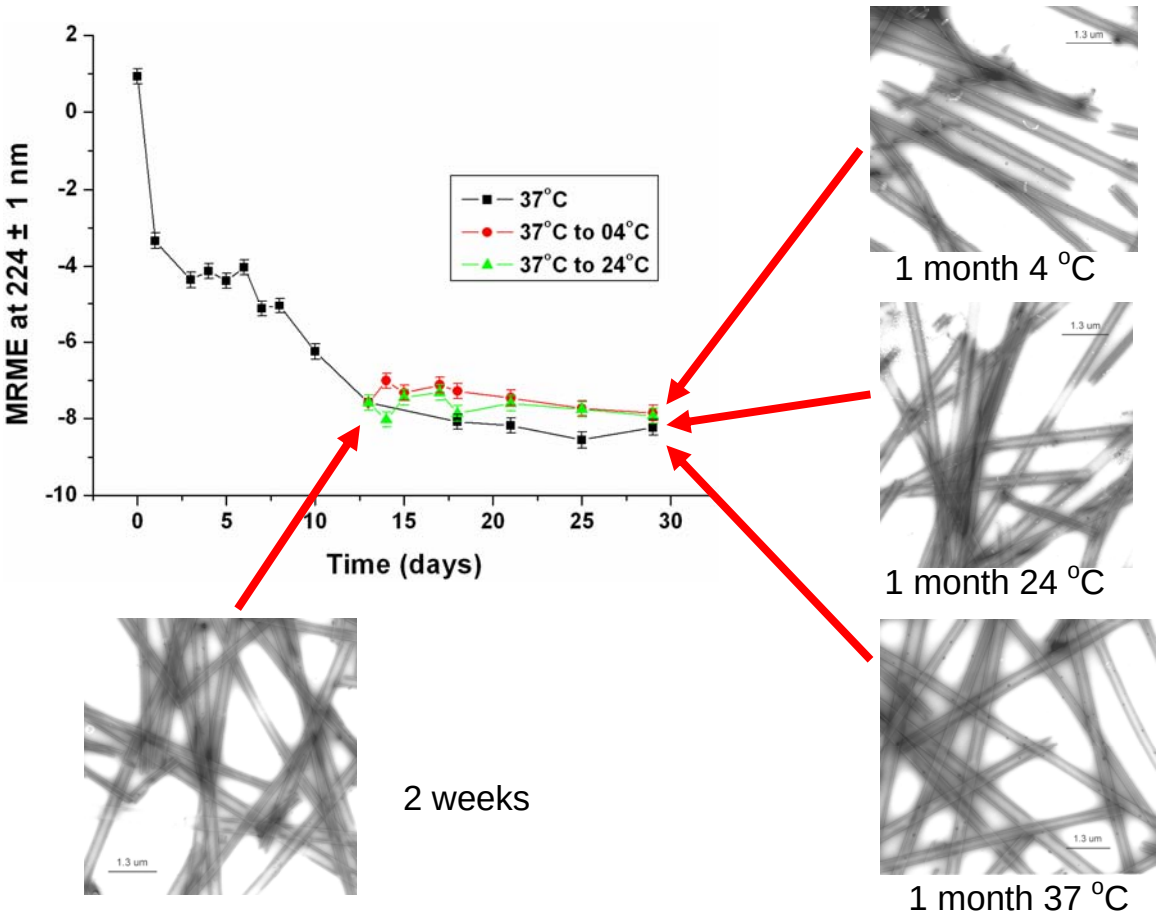

Figure 2.5. The plot of CD intensity at 224 nm for the first four weeks. After incubating at 37 °C for two weeks, sample was divided into three and incubated at three different temperatures, respectively. TEM images were taken after two weeks and after four weeks.

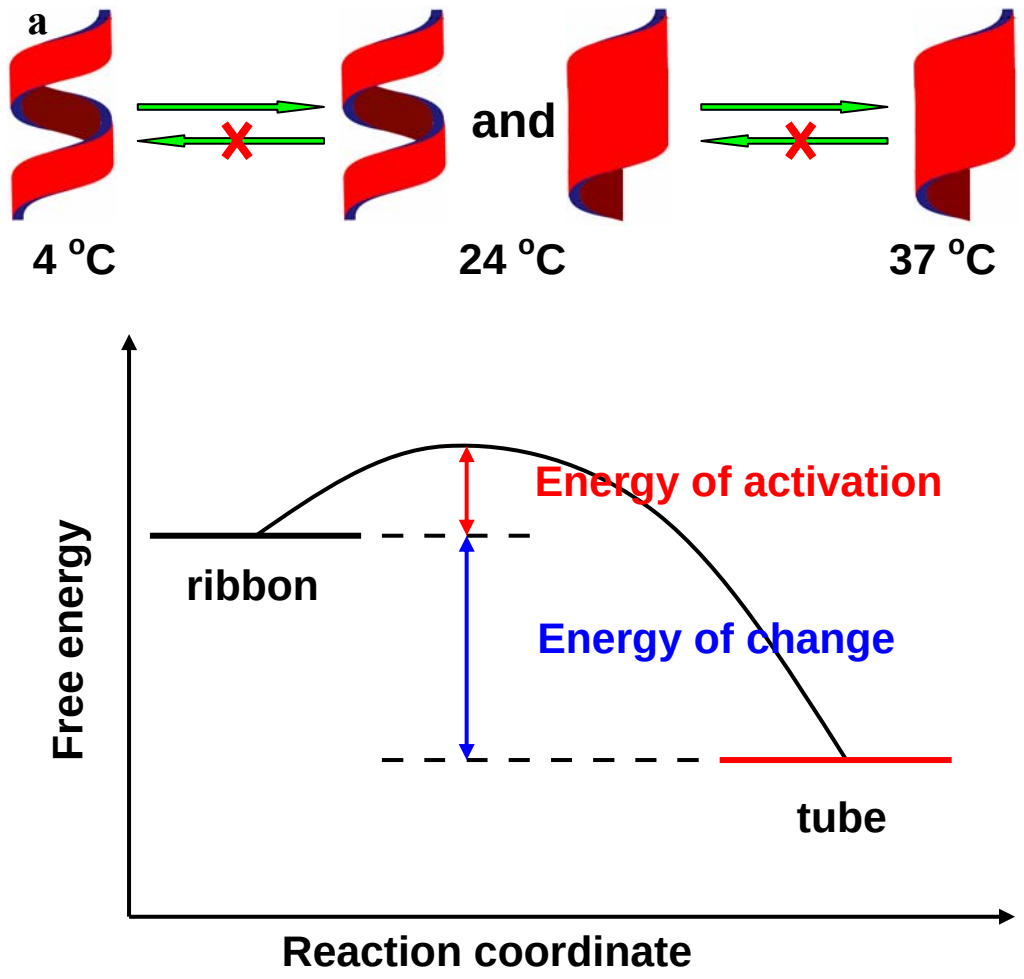

Figure 2.6. (a) Scheme of the morphology change between different temperatures. (b) Energy diagram of the change between ribbons and tubes.

Peptide arrangement in Zinc induced peptide nanotube

For Aβ(13-21)K16A peptide, previous ssNMR and FT-IR studies show that peptides form amyloid ribbons with anti-parallel and out-of-register arrangements (Dong 2006). The exact details at the out-of-register arrangement is still unknown, but ssNMR experiments can be performed to further determine the peptide orientation by directly measuring the distance between selected ^{13}C and ^{15}N isotopes in a $^{13}C\{^{15}N\}$ REDOR

measurement. When there is no pulses on ^{15}N, ^{13}C spectrum, named as S_0, shows very slow decay. When pulses are applied to ^{15}N to introduce the dipole coupling between ^{13}C and ^{15}N, ^{13}C spectrum will show increase decay if ^{13}C is close to the ^{15}N. The spectrum difference before and after ^{15}N pulses is called ΔS. Therefore, only when the ^{13}C is close to a ^{15}N, it will appear in the ΔS spectrum. The decay rate of $\Delta S/S_0$ is directly related with the distance between them, the steeper the slope, the shorter the distance. Three different labeled peptides, [^{15}N]A16-[1-^{13}C]F19, [^{15}N]A16-[1-^{13}C]F20, and [^{15}N]L17-[1-^{13}C]F20, have been synthesized and purified (Figure 2.7).

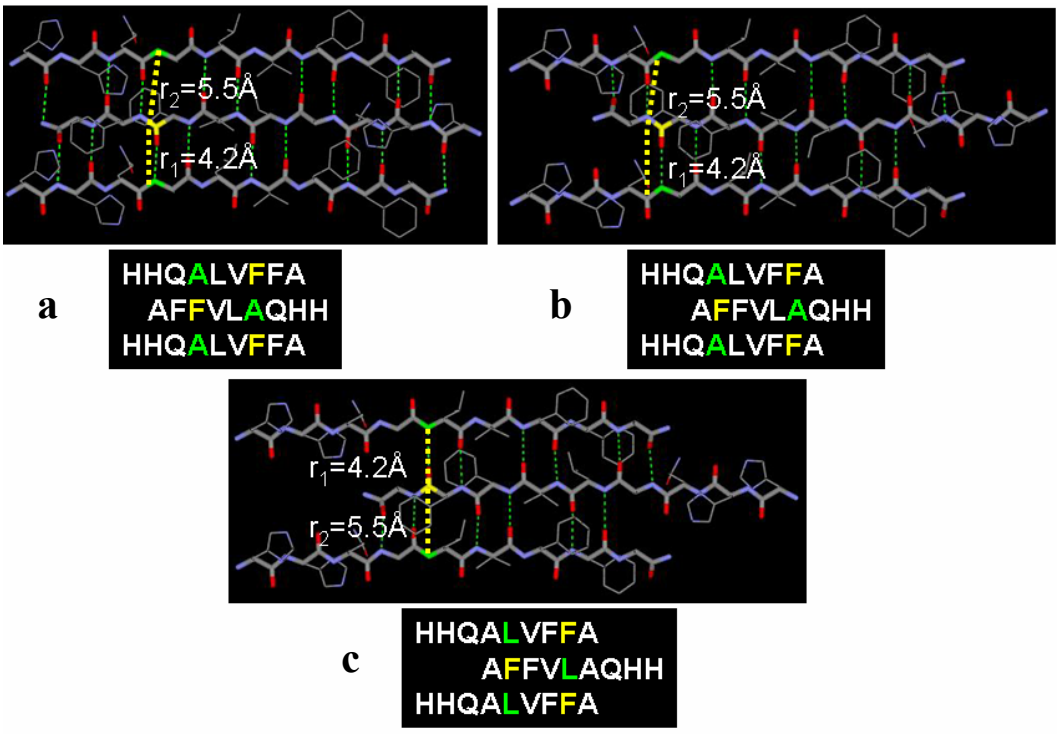

Figure 2.7. Schematic representation of the relative position of ^{13}C labels (yellow) and ^{15}N labels (green) in anti-parallel (a) one residue out-of-registry for [^{15}N]A16-[1-^{13}C]F19, (b) two residue out-of-registry for [^{15}N]A16-[1-^{13}C]F20, and (c) three residue out-of-registry arrangements for [^{15}N]L17-[1-^{13}C]F20.

To do the solid state NMR, the most important step is to freeze and dry the sample. The structure of the amyloid must be as intact as possible during this process. The stability of the peptide nanotubes has been studied during the cryo- and lyo- processes. As shown in Figure 2.8a, mature assemblies were pelleted and lyophilized. Precipitates were pelleted and re-suspended in 5 mL of cryo- and lyo-protectant solution (Wang 2000; Studelska et al. 2003) , containing 30 mM trehalose, 0.67 mg/ml dextran (81.5 kDa and 488 kDa) and 1% PEG-8000, and then quick frozen in -40 °C acetonitrile/dry ice bath. Finally, sample was put into lyophilizer. Circular dichroism (CD) signals and TEM images were monitored at different stages in cryo- and lyo- processes (Figure 2.8b, Figure 2.8c). As shown in Figure 2.8b, CD signals decrease a lot during the cryo- and lyo- processes. After lyophilization, CD signals in both 199 nm and 221 nm disappear. TEM images are also consistent with the CD results. Undestroyed peptide nanotubes can be visualized during the first three steps, and only large aggregates can be visualized after lyophilization. In summary, peptide nanotubes will be destroyed during lyophilization and need to be protected during the cyro- and lyo- processes before the ssNMR experiments.

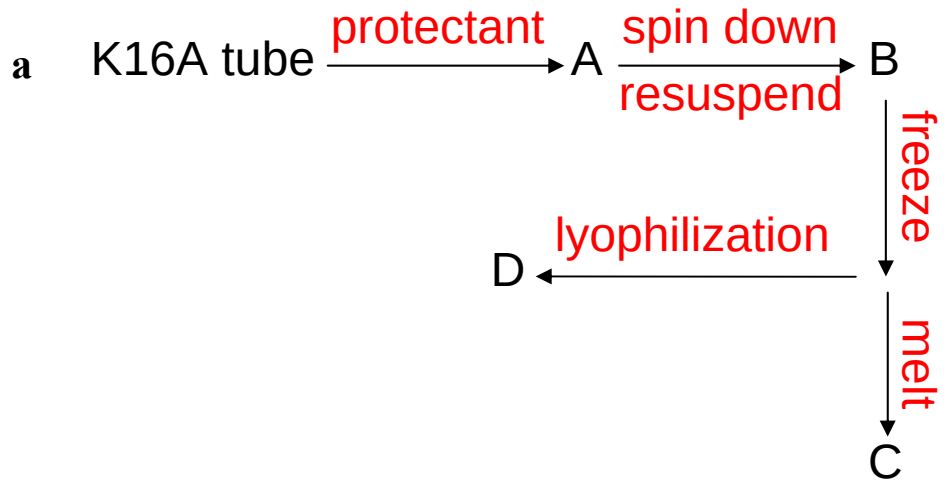

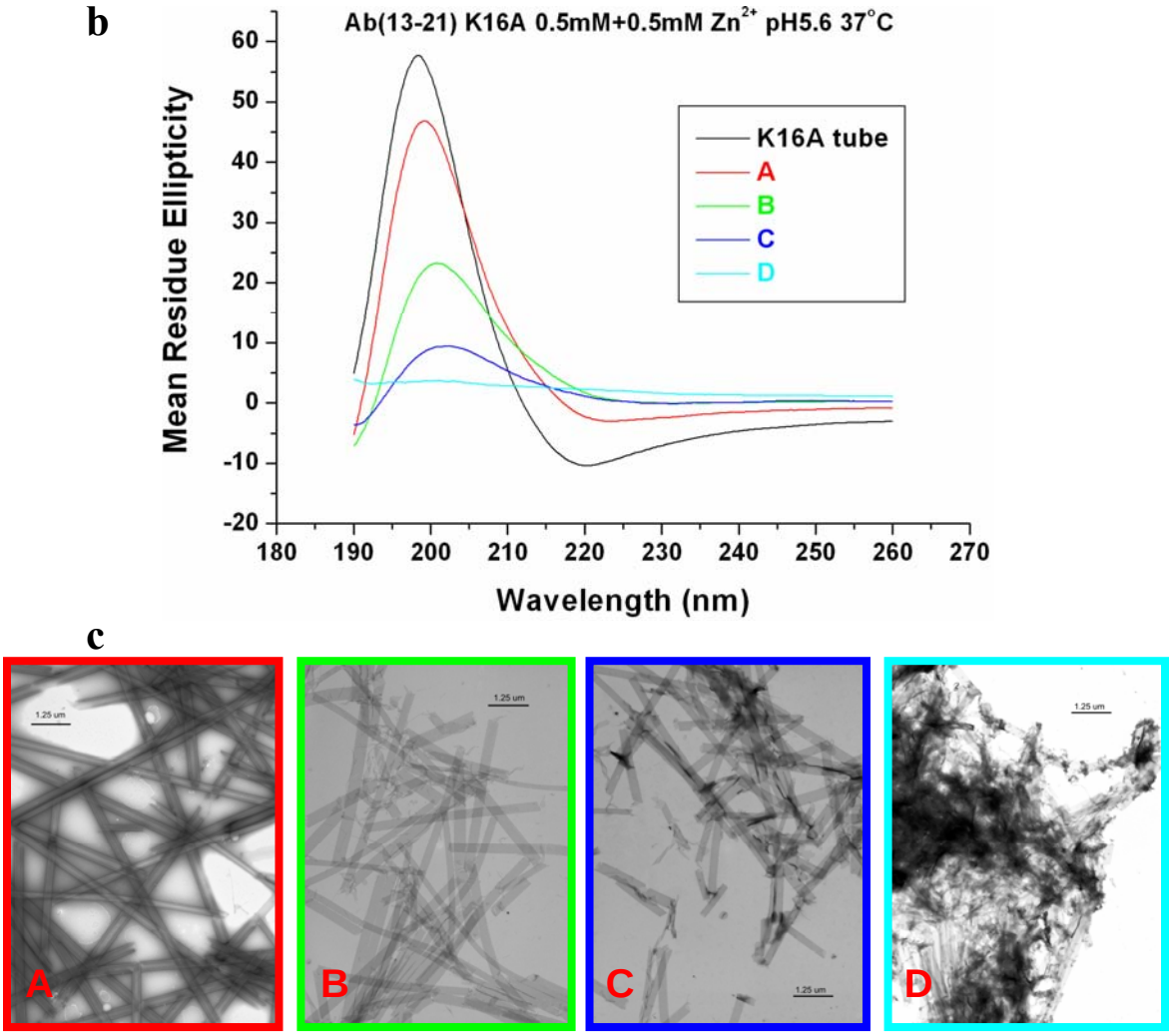

Figure 2.8. Cryo- and lyo- processes of 0.5 mM Aβ(13-21)K16A in 25 mM MES buffer at pH 5.6 at 37 ^{o}C in the presence of 0.5 mM Zn^{2+}. (a) Scheme illustration of cryo- and lyo- processes; (b) circular dichroism (CD) spectra at different stages of cryo- and lyo- processes; (c) TEM images at different stages of cryo- and lyo- processes.

To protect the samples from denaturation caused by freezing and lyophilization, some efforts were made to bundle the mature peptide nanotubes. For Aβ(16-22) peptide, at pH 2 in 40 % acetonitrile, peptides can self assemble into peptide nanotubes. The negatively charged sulfate ions interact with the positively charged tube surfaces to

bundle individual tubes into well-aligned macrofibers. It is found that the sulfate-induced peptide nanotube bundles can withstand the harsh conditions of lyophilization (Kun 2007).

For Aβ(13-21)K16A peptide, at pH 5.6, because of the protonated free N-terminal amino groups, self-assembled peptide nanotubes also have positively charged tube surfaces. On the other hand, zinc ions, which coordinate to two His groups, are also located at the surfaces of the peptide nanotubes. Based on these, there are two strategies to bundle the peptide nanotubes (Figure 2.9). At first, several anions can be used to interact with positively charged tube surfaces to bundle the peptide nanotubes. Secondly, due to the existence of the zinc ions, several ligands can also be designed to coordinate to zinc ions and draw different tubes together and bundle the peptide nanotubes.

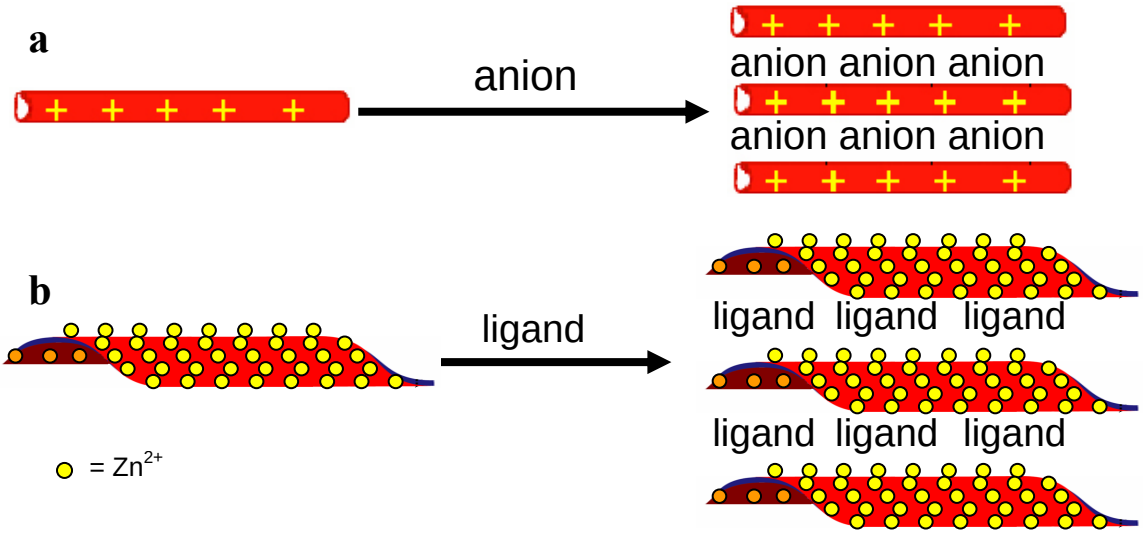

Figure 2.9. Two strategies to bundle the peptide nanotubes. (a) anions interact with positively charged tube surfaces to bundle the peptide nanotubes; (b) ligands chelate to zinc ions to bundle the peptide nanotubes.

Salt-induced precipitation is widely used for purification of charged proteins and

can also precipitate amyloid fibrils (Scopes 1994; Fraser 1992). The precipitation strongly depends on the ion's position in the Hofmeister series, in which the anions and cations on the left can keep the protein native structure very well. In Hofmeister series, SO_4^{2-} is efficient for precipitating positively charged proteins. Aβ(16-22) nanotubes can be bundled into well-aligned macrofibers with the addition of SO_4^{2-} (Kun 2007). At pH 5.6, SO_4^{2-} bears two negative charges (H_2SO_4, pKa1 = -3 and pKa2 = 2). At first, peptides self assembled in MES buffer at 37 ^oC. Once SO_4^{2-} was added into mature Aβ(13-21)K16A peptide nanotubes to a final concentration 20 mM, visible white precipitates formed immediately. As shown in Figure 2.10 by TEM images, SO_4^{2-} aggregates the peptide nanotubes and also somewhat destroyes the tubular structure. Being different with Aβ(16-22), SO_4^{2-} cannot bundle the peptide nanotubes formed by Aβ(13-21)K16A.

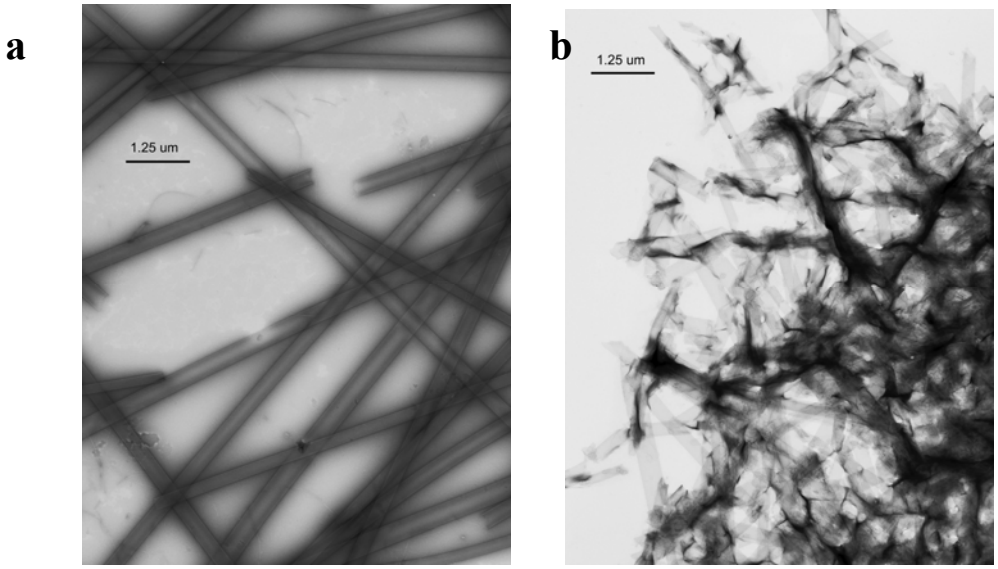

Figure 2.10. (a) TEM image of 0.5 mM Aβ(13-21)K16A in 25 mM MES buffer at pH 5.6 at 37 ^oC in the presence of 0.5 mM Zn^{2+} after two weeks; (b) With the addition of 20 mM SO_4^{2-}, other conditions are the same with (a).

Since SO_4^{2-} cannot bundle peptide nanotubes, several ligands were applied to bundle the peptide nanotubes according to the second strategies. The first ligand I chose is ethylenediamine tetraacetic acid (EDTA) (Figure 2.11a). As shown in Figure 2.11b, with the addition of 1 mM EDTA into mature peptide nanotube solution, CD signals in around 199 nm and 221 nm both decrease dramatically. After three days' incubation, positive peak disappeared, and the negative beta sheet signal also decreased a lot. TEM images are also consistent with the CD results. With the addition of 1 mM EDTA, peptide nanotubes began to dissemble and form amyloid fibrils. After three days, almost all peptide nanotubes disappeared and formed amyloid fibrils (Figure 2.11c and Figure 2.11d). All these results demonstrate that EDTA cannot bundle the peptide nanotubes. A possible explanation is that EDTA is a very strong chelate. EDTA has six atoms which can coordinate to zinc ions. As a result, EDTA and Zn^{2+} can interact with each other to form an octahedral compound. Also, zinc ions in peptide nanotubes will be pulled out, and peptide nanotubes will break down and finally form amyloid fibrils. Based on these, other ligands need to be designed to bundle the peptide nanotubes. There are three important things that we need to concern about. At first, the ligands should have two groups which can coordinate to two different zinc ions from different peptide nanotubes. Secondly, the structures of ligands should have some rigidity so that two groups would not coordinate to a single zinc ion. For this purpose, the distances between two coordination groups should be short. Finally, the ligands should have good solubility in MES buffer solution. Several ligands, such as 1,2-ethanedithiol, Hydroquinone. Terephthalic acid, and 1,4-Benzenedimethanethiol have been chosen to bundle the peptide nanotubes (Figure 2.12).

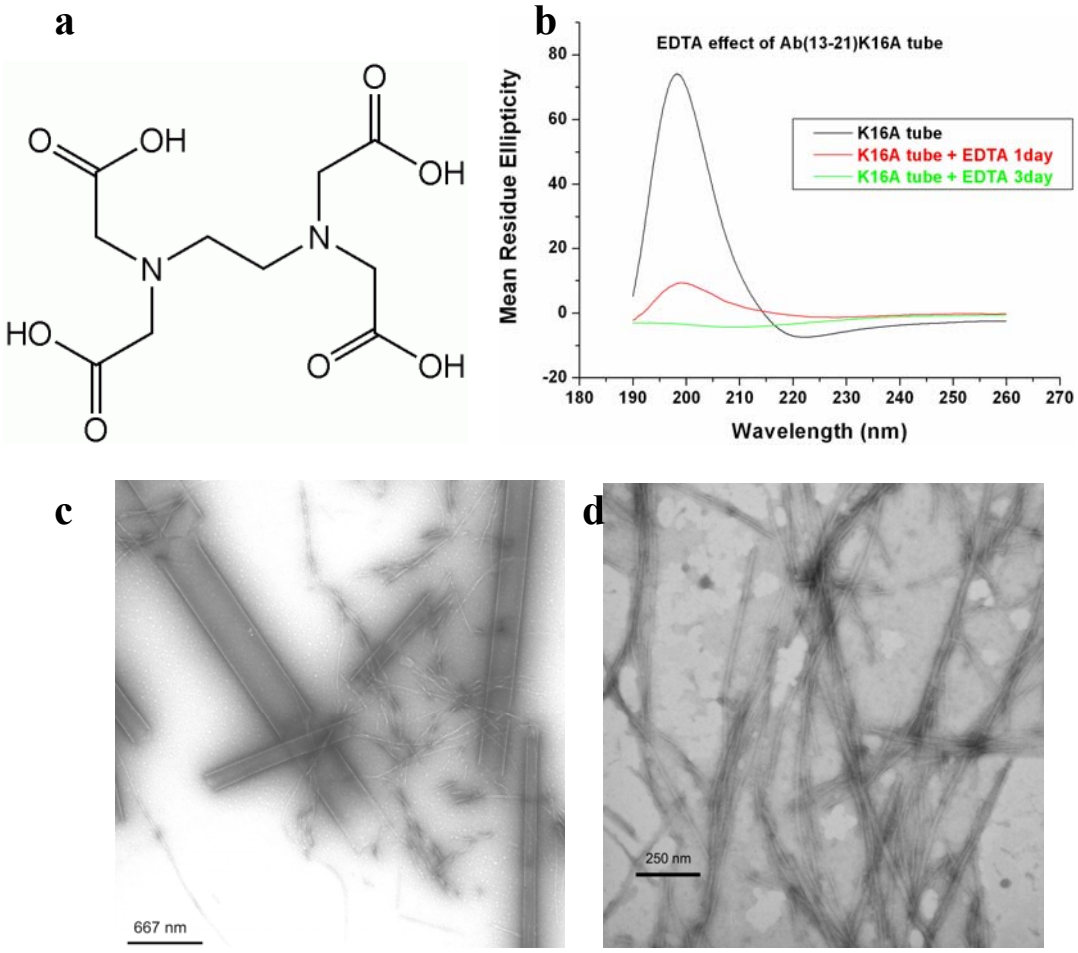

Figure 2.11. EDTA effect on the Zn^{2+}-induced Aβ(13-21)K16A peptide nanotubes at 37 ^{o}C. (a) The structure of EDTA; (b) circular dichroism (CD) spectra of Aβ(13-21)K16A peptide nanotubes before and after the addition of 0.5 mM EDTA; (c) TEM image taken one day after the addition of 0.5 mM EDTA; (d) TEM image taken three days after the addition of 0.5 mM EDTA.

The first ligand I tried is terephthalic acid (pKa1 = 3.51; pKa2 = 4.82). Once 0.25 mM terephthalic acid was added into mature Aβ(13-21)K16A peptide nanotubes, no visible change was observed from solution. As shown in Figure 2.13a, with the addition of 0.25 mM terephthalic acid, CD signals in around 199 nm and 221 nm both decrease

dramatically. As shown in Figure 2.13b by TEM image, terephthalic acid aggregates the peptide nanotubes and also somewhat destroyes the tubular structure. As a result, terephthalic acid cannot bundle the peptide nanotubes.

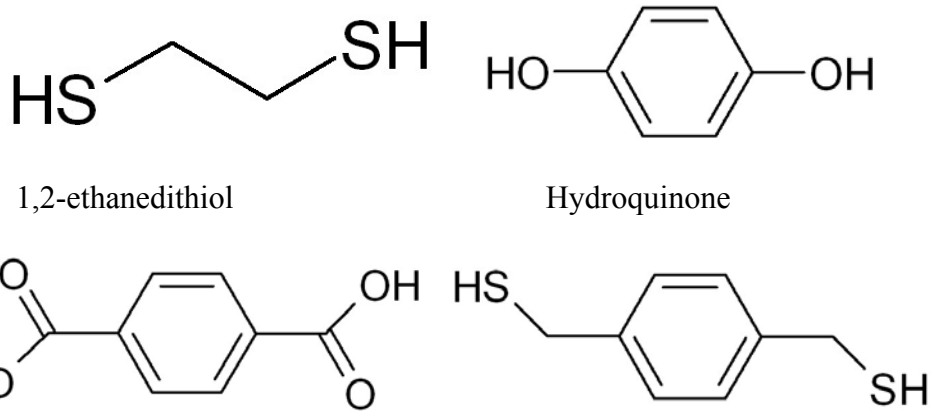

1,2-ethanedithiol Hydroquinone

Terephthalic acid 1,4-Benzenedimethanethiol

Figure 2.12. Structures of 1,2-ethanedithiol, hydroquinone, terephthalic acid, and 1,4-benzenedimethanethiol.

Once 0.25 mM hydroquinone was added into mature Aβ(13-21)K16A peptide nanotubes, both CD and TEM images showed big difference with hydroquinone. As shown in Figure 2.14a, both signals in around 199 nm and 221 nm show no big difference before and after the addition of 0.25 mM hydroquinone. TEM image also shows the dispersed peptide nanotubes (Figure 2.14b). It suggests that there is no direct interaction between hydroquinone and peptide nanotubes. The possible explanation is that hydroquinone can not coordinate to zinc ions at pH 5.6. At pH 5.6, hydroquinone (pKa1 = 3.51; pKa2 = 4.82) is protonated. It is difficult for the oxygens in hydroxyl group to coordinate to zinc ions.

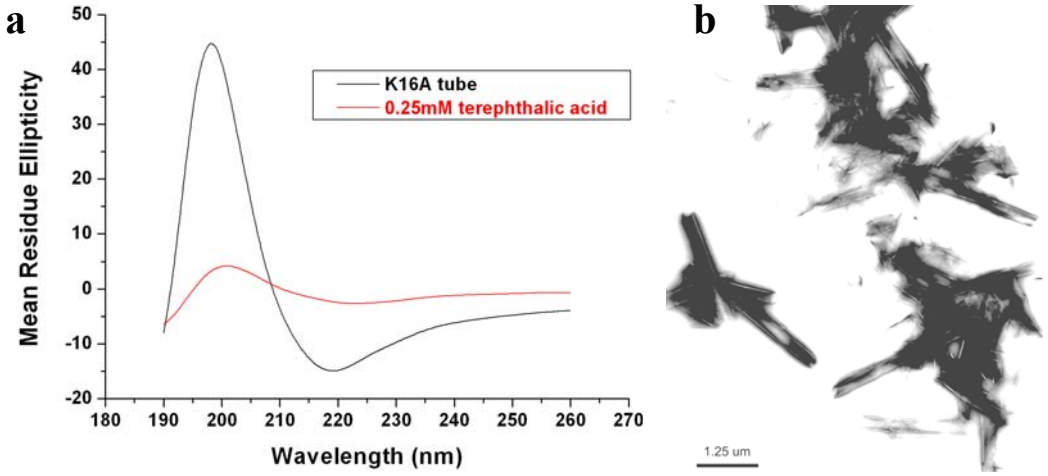

Figure 2.13. Terephthalic acid effect on the Zn^{2+}-induced Aβ(13-21)K16A peptide nanotubes at 37 ^{o}C. (a) circular dichroism (CD) spectra of Aβ(13-21)K16A peptide nanotubes before and after the addition of 0.25 mM terephthalic acid; (b) TEM image taken three days after the addition of 0.25 mM terephthalic acid.

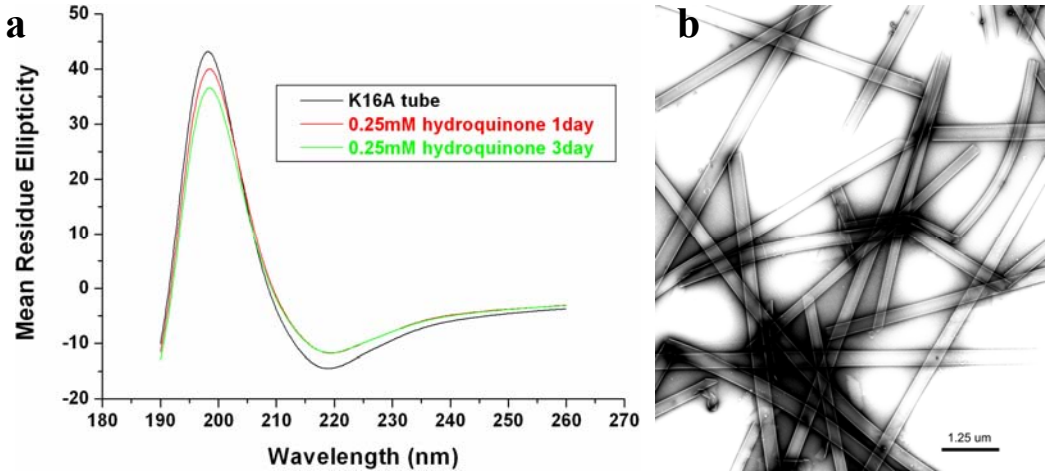

Figure 2.14. Hydroquinone effect on the Zn^{2+}-induced Aβ(13-21)K16A peptide nanotubes at 37 ^{o}C. (a) circular dichroism (CD) spectra of Aβ(13-21)K16A peptide nanotubes before and after the addition of 0.25 mM hydroquinone; (b) TEM image taken three days after the addition of 0.25 mM hydroquinone.

Once 0.25 mM 1,2-ethanedithiol was added into mature Aβ(13-21)K16A peptide nanotubes at 37 ^{o}C, no visible change was observed from solution. As shown in Figure 2.15a, with the addition of 0.25 mM 1,2-ethanedithiol, the negative beta sheet signals at around 221 nm decrease, and the positive signals at 199 nm only decrease a little bit. TEM images show no big difference before and after the addition of 1,2-ethanedithiol (Figure 2.15b).

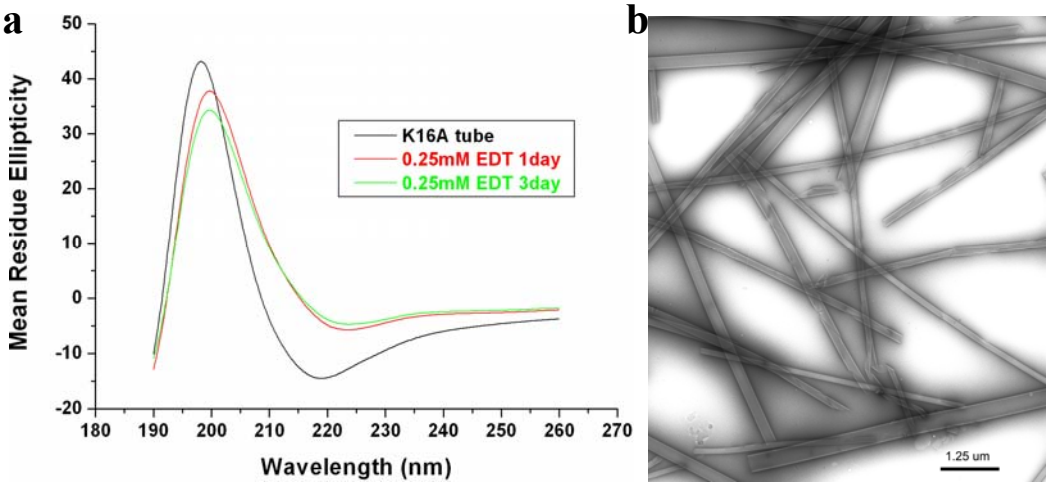

Figure 2.15. 1,2-ethanedithiol effect on the Zn^{2+}-induced Aβ(13-21)K16A peptide nanotubes at 37 ^{o}C. (a) circular dichroism (CD) spectra of Aβ(13-21)K16A peptide nanotubes before and after the addition of 0.25 mM 1,2-ethanedithiol; (b) TEM image taken three days after the addition of 0.25 mM 1,2-ethanedithiol.

Similar results were also found when 0.25 mM 1,4-Benzenedimethanethiol was added into mature peptide nanotubes at 37 ^{o}C. As shown in Figure 2.16a, with the addition of 0.25 mM 1,4-Benzenedimethanethiol, the negative beta sheet signals at around 221 nm decrease, and the positive signals at 199 nm only decrease a little bit, which is similar to 1,2-ethanedithiol. TEM images show no big difference before and

after the addition of 1,4-Benzenedimethanethiol (Figure 2.16b).

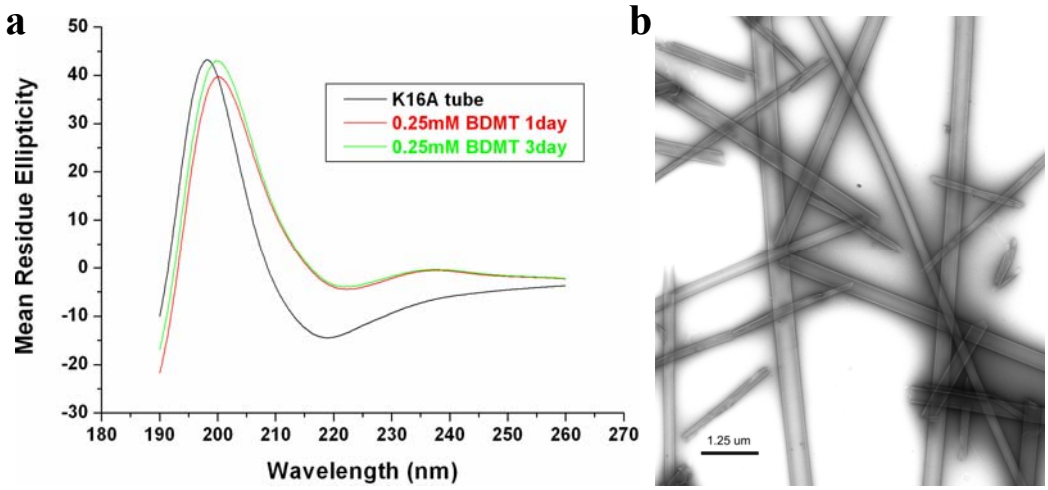

Figure 2.16. 1,4-Benzenedimethanethiol effect on the Zn^{2+}-induced Aβ(13-21)K16A peptide nanotubes at 37 ^{o}C. (a) circular dichroism (CD) spectra of Aβ(13-21)K16A peptide nanotubes before and after the addition of 0.25 mM 1,4-Benzenedimethanethiol; (b) TEM image taken three days after the addition of 0.25 mM 1,4-benzenedimethanethiol.

The results of the bundling experiments are summarized in Table 2.1. All of these anions and ligands cannot bundle the Aβ(13-21)K16A peptide nanotubes. While the addition of sulfate and terephthalic acid will aggregate and untwist the peptide nanotubes, in the presence of EDTA, the peptide nanotubes dissemble and form amyloid fibrils. In contrast, in the presence of hydroquinone, 1,2-ethanedithiol and 1,4-benzenedimethanethiol, peptide nanotubes will not aggregate or be destroyed. At pH 5.6, sulfate, EDTA, and terephthalic acid contain two negative charges, and hydroquinone, 1,2-ethanedithiol and 1,4-benzenedimethanethiol are neutral. As a result, anions and negative-charged molecules aggregate and potentially destabilize peptide nanotubes. On

the other hand, in the presence of strong chelate, such as EDTA, peptide nanotubes will dissemble and finally form amyloid fibrils.

Table 2.1. A summary of bundling experiments.

	SO_4^{2-}	EDTA	Terephthalic acid	Hydroquinone	1,2-ethanedithion	1,4-Benzenedimethanethiol
charges	-2	-2	-2	0	0	0
No. of coordination groups	2	4-6	2	2	2	2
CD signal	decrease	decrease	decrease	no obvious change	no obvious change	no obvious change
TEM image	aggregate & untwist	form fibril	aggregate & untwist	no visible change	no visible change	no visible change

Now, the question is why these anions and ligands cannot bundle the peptide nanotubes. There're two explanations. At first, zinc coordination in Aβ(13-21)K16A peptide nanotubes is fragile and easily destroyed by some anions and chelates. Under these conditions, zinc ions will interact with ligands and be pulled out to form more stable complexes. Several other weaker ligands might be useful. The second possible reason is that zinc ions are not on the surface of the Aβ(13-21)K16A peptide nanotubes. Under this condition, ligands cannot enter the peptide nanotubes and interact with zinc ions. As a result, the bundling of the peptide nanotubes can only be achieved by interaction between anions and the positively charged tube surfaces. Under these conditions, other anions from the Hofmeister Series should be tested to bundle the peptide nanotubes.

Stability of Zn^{2+}-induced Aβ(13-21)K16A peptide nanotubes

In order to study the physical stability of Zn^{2+}-induced Aβ(13-21)K16A peptide

nanotubes, two different solvents, methanol and acetonitrile, have been used for peptide self-assembly.

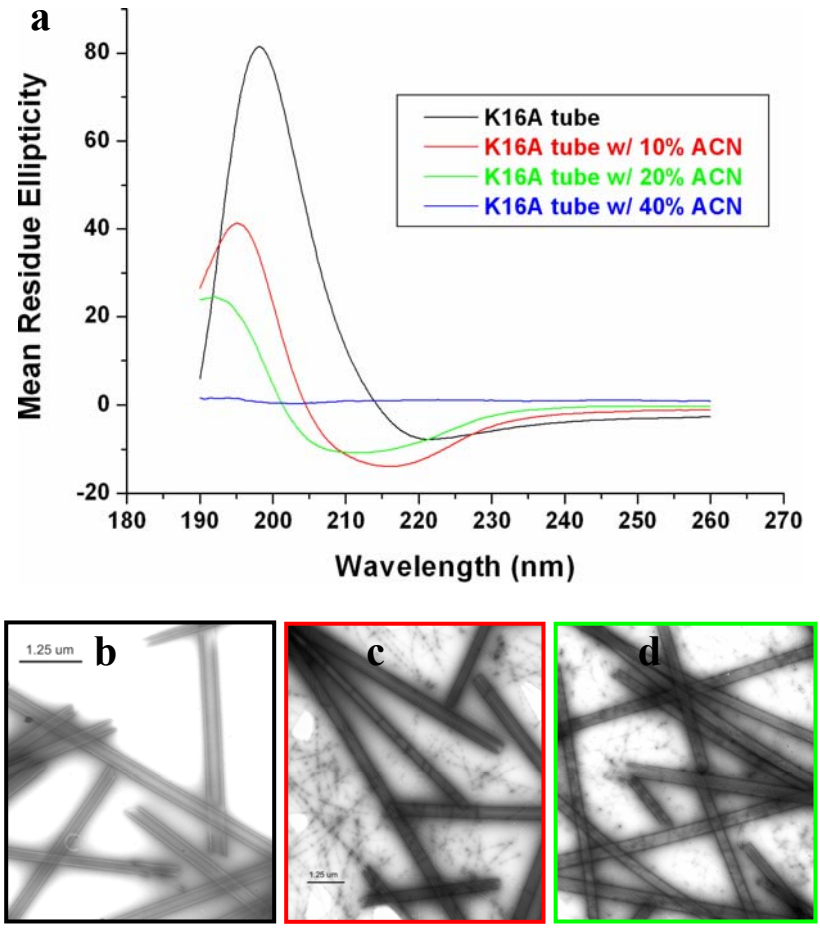

Figure 2.17. Acetonitrile effect on the preformed Zn^{2+}-induced Aβ(13-21)K16A peptide nanotubes at 37 ^{o}C. (a) circular dichroism (CD) spectra of Aβ(13-21)K16A peptide nanotubes at different acetonitrile concentrations; (b) TEM image at 0 % acetonitrile; (c) TEM image at 10 % acetonitrile; (d) TEM image at 20 % acetonitrile; no visible structure from TEM at 40 % acetonitrile.

At first, different amounts of acetonitrile have been added into preformed Zn^{2+}-induced Aβ(13-21)K16A peptide nanotubes at 37 ^{o}C. As is shown in Figure 2.17a, with

the increasing of acetonitrile concentration, the negative beta sheet CD signals and the positive signals have some blue shift, and the positive peaks decrease a lot. Increasing acetonitrile concentration will also change morphology (Figure 2.17b, 2.17c, and 2.17d). When adding 10 % and 20 % acetonitrile, peptide nanotubes will dissemble and form some amyloid fibrils (Figure 2.17c and 2.17d). From TEM images, a mixture of peptide nanotubes and fibrils can be visualized. When acetonitrile concentration increases to 40 %, no visible structure can be obtained. Under this condition, peptide nanotubes melt completely and don't form amyloid fibrils. All these experiments indicate that acetonitrile destabilizes the Aβ(13-21)K16A peptide nanotubes.

Different amounts of methanol, 10 %, 20 %, and 40 %, were also added into preformed Zn^{2+}-induced Aβ(13-21)K16A peptide nanotubes at 37 ^{o}C. As shown in Figure 2.18a, with the elevated methanol concentration, both the negative beta sheet signals and positive signals have some blue shifts. The positive peak will decrease significantly with the increased methanol concentration. From the TEM images, it is clearly that methanol destabilizes peptide nanotubes (Figure 2.18b, 2.18c, 2.18d, and 2.18e). When adding 10 % methanol, peptide nanotube began to dissemble and finally form some amyloid fibrils (Figure 2.18c). TEM image shows a mixture of peptide nanotubes and fibrils. When the methanol concentration increases to 20 % and 40 %, almost all peptide nanotubes dissemble and form amyloid fibrils (Figure 2.18d and 2.18e). TEM images only show amyloid fibrils and no nanotubes. Similarly, all these experiments indicate that methanol destabilizes the Aβ(13-21)K16A peptide nanotubes.

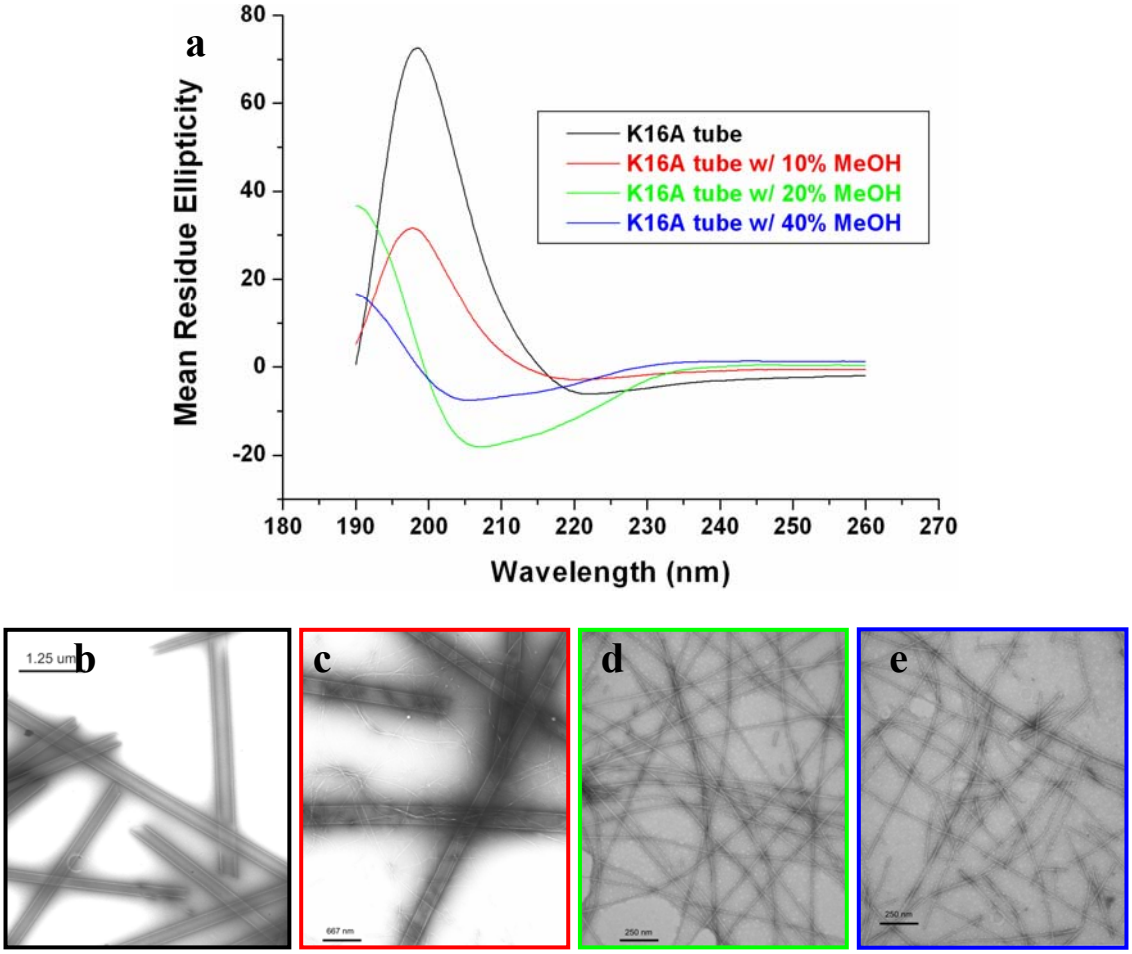

Figure 2.18. Methanol effect on the preformed Zn^{2+}-induced Aβ(13-21)K16A peptide nanotubes at 37 ^{o}C. (a) circular dichroism (CD) spectra of Aβ(13-21)K16A peptide nanotubes at different methanol concentrations; (b) TEM image at 0 % methanol; (c) TEM image at 10 % methanol; (d) TEM image at 20 % methanol; (e) TEM image at 40 % methanol.

Previously, different amounts of acetonitrile and methanol were added into preformed Zn^{2+}-induced Aβ(13-21)K16A peptide nanotubes. Next, a series of 0.5 mM Aβ(13-21)K16A samples were prepared in 25 mM MES buffer at pH 5.6 in the presence of 0 %, 20 %, and 40 % methanol with 0.5 mM Zn^{2+} at 37 ^{o}C. As is shown in Figure

2.19a, 2.19c, and 2.19e, at higher concentration of methanol, both the negative beta sheet signals and positive signals have some blue shifts. The higher the methanol concentration, the more shift to blue. TEM images also demonstrate that higher concentration of methanol inhibits the formation of peptide nanotubes. As is shown in Figure 2.19b, in 0 % methanol, peptides self assemble into peptide nanotubes. In contrast, in 20 % methanol solution, peptides finally self assemble into a mixture of nanotubes and fibrils (Figure 2.19d). When the concentration of methanol increases to 40 %, almost all peptides self assemble into amyloid fibrils, and only a very small piece of ribbon can be visualized by TEM (Figure 2.19f). All these experiments also confirm that methanol inhibits the formation of peptide nanotubes.

A series of 0.5 mM Aβ(13-21)K16A samples were also allowed to self assemble in 25 mM MES buffer at pH5.6 in the presence of 0 %, 20 %, and 40 % acetonitrile with 0.5 mM Zn^{2+} at 37 ^{o}C. As is shown in Figure 2.20, in 20 % acetonitrile solution, peptides finally self assembled into amyloid fibril, and no peptide nanotubes were observed. When the concentration of acetonitrile increases to 40 %, peptides cannot self assemble, and no visible structure can be onserved.

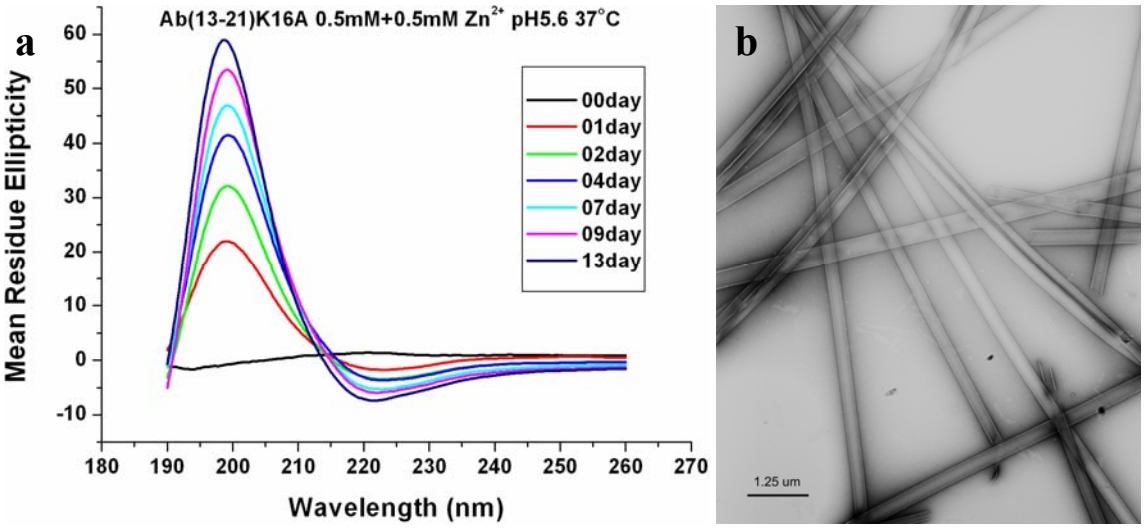

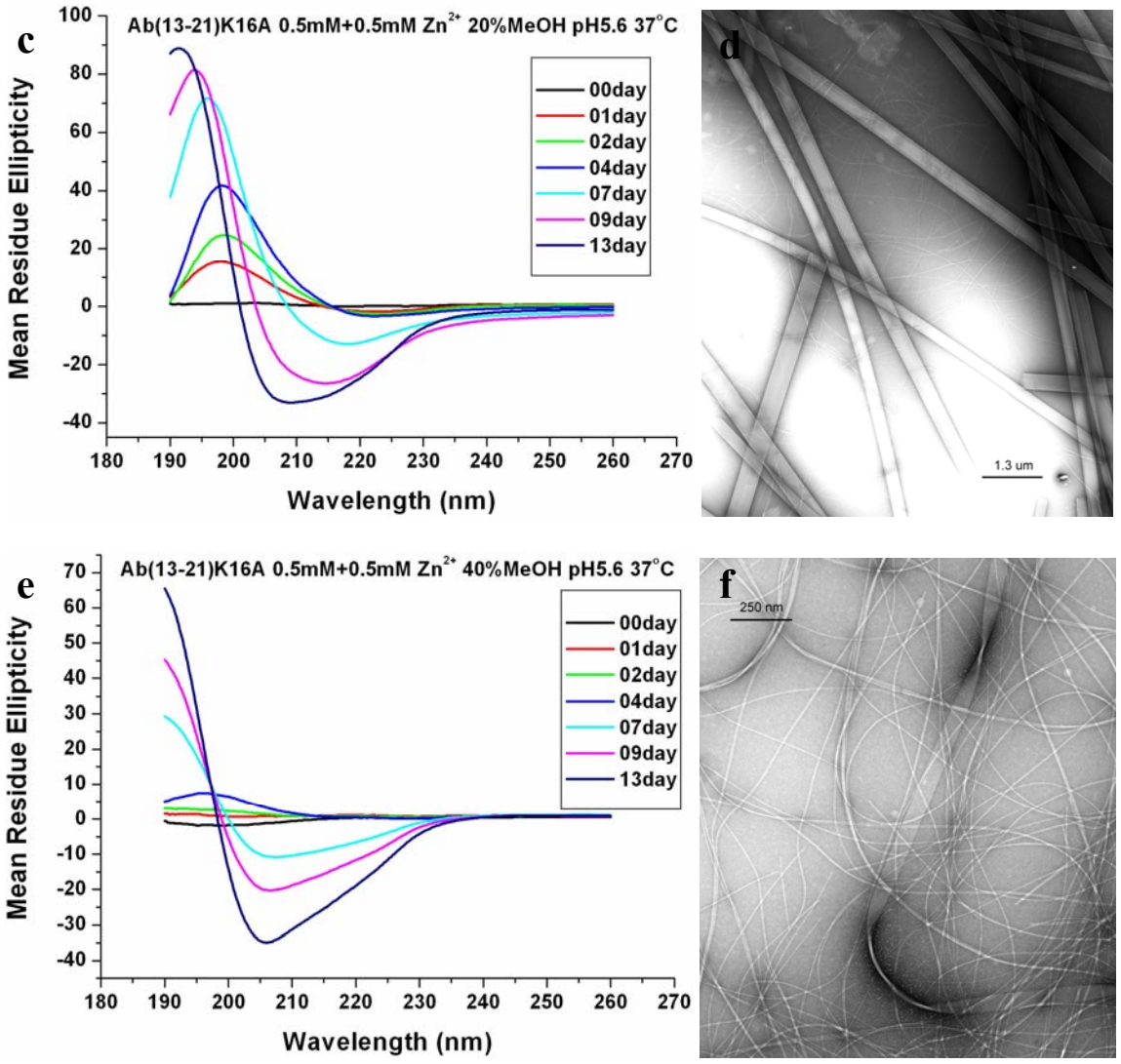

Figure 2.19. Methanol effect on Aβ(13-21)K16A peptide self-assembly in the presence of Zn^{2+} at 37 ^{o}C. (a) CD spectra over time of 0.5 mM Aβ(13-21)K16A in the presence of Zn^{2+} with 0 % methanol; (b) TEM image at 0 % methanol after two weeks; (c) CD spectra over time of 0.5 mM Aβ(13-21)K16A in the presence of Zn^{2+} with 20 % methanol; (d) TEM image at 20 % methanol after two weeks; (e) CD spectra over time of 0.5 mM Aβ(13-21)K16A in the presence of Zn^{2+} with 40 % methanol; (f) TEM image at 40 % methanol after two weeks.

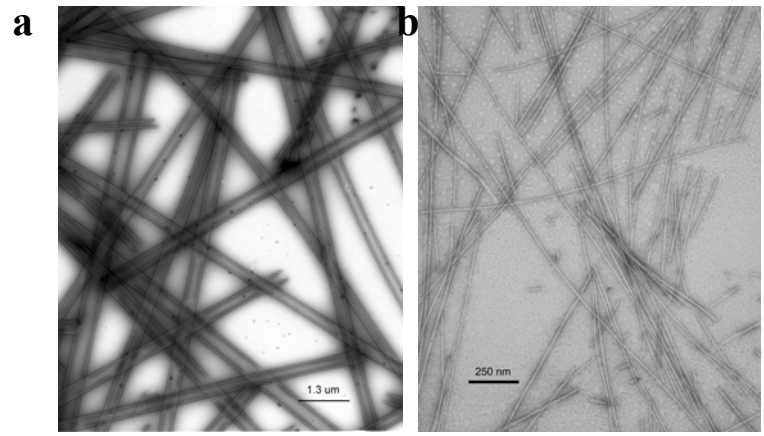

Figure 2.20. Acetonitrile effect on Aβ(13-21)K16A peptide self-assembly in the presence of Zn^{2+} at 37 ^{o}C. (a) TEM image at 0 % acetonitrile after two weeks; (b) TEM image at 20 % acetonitrile after two weeks; no visible structure from TEM at 40 % acetonitrile after two weeks.

These studies show that peptide nanotubes are not stable at higher concentration of methanol and acetonitrile at 37 ^{o}C. The solvent effects on the peptide self-assembly at different temperatures have also been studied. A series of 0.5 mM Aβ(13-21)K16A samples were prepared to self assemble in 25 mM MES buffer at pH 5.6 in the presence of 20 % acetonitrile with 0.5 mM Zn^{2+} at 4 ^{o}C, 24 ^{o}C, and 37 ^{o}C. As is shown in Figure 2.21a, with the increasing temperature, both the negative beta sheet signals and positive signals have some blue shifts. The higher the temperature, the more shift to blue. TEM images also show big differences. At 4 ^{o}C, peptides formed a mixture of helical ribbons and nanotubes (Figure 2.21b). There was no fibril formation. At 24 ^{o}C, peptides formed a mixture of fibrils, ribbons, and nanotubes (Figure 2.21c). At 37 ^{o}C, almost all peptides self assembled into amyloid fibrils. There's no ribbon or nanotubes formation (Figure 2.21d). All these results indicate that zinc induced peptide ribbons or nanotubes are more

stable at lower temperature in the presence of acetonitrile.

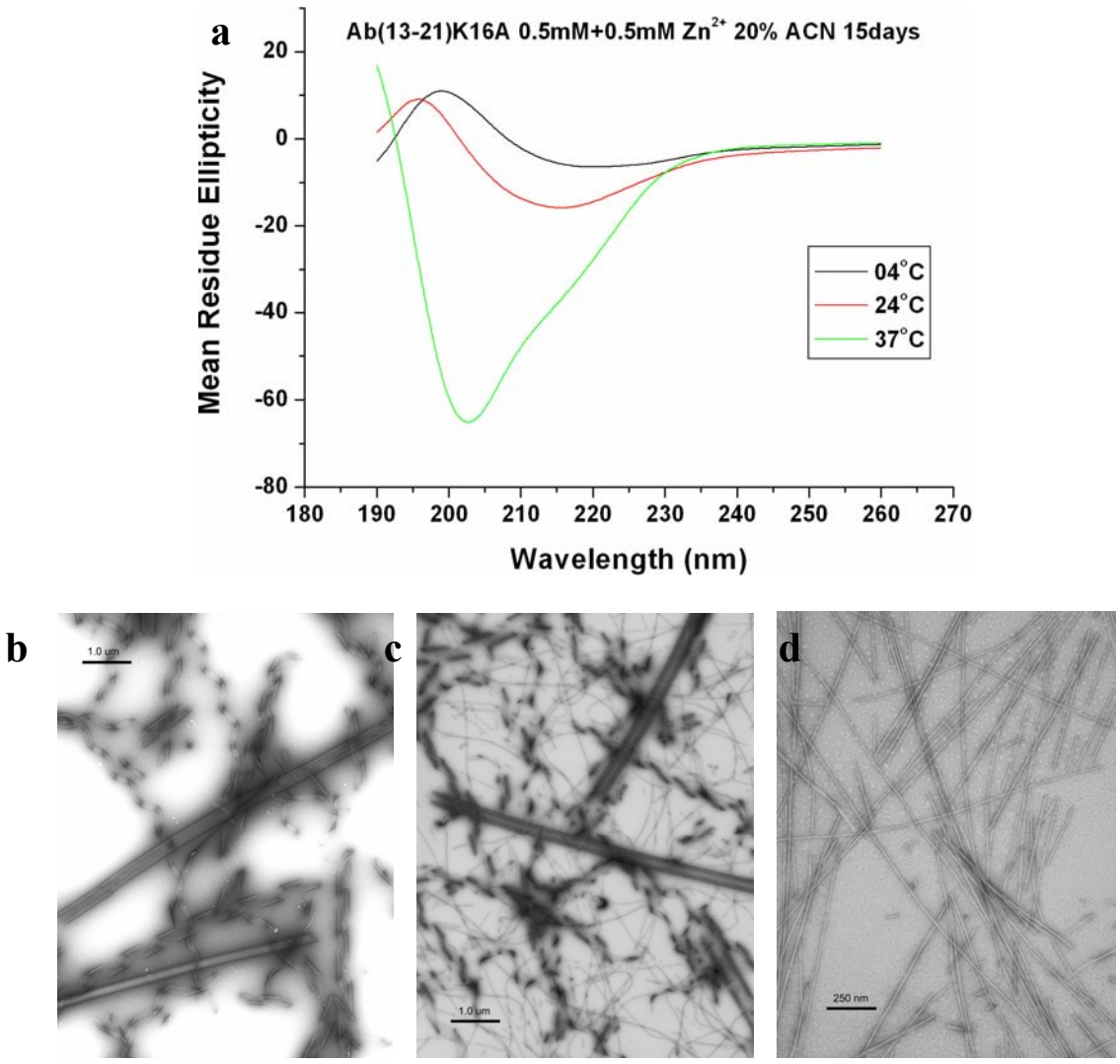

Figure 2.21. Temperature effect on Aβ(13-21)K16A peptide self-assembly in the presence of 20% acetonitrile with 0.5 mM Zn^{2+}. (a) circular dichroism (CD) spectra of Aβ(13-21)K16A peptide self-assembly at different temperature; (b) TEM image at 4 ^{o}C methanol; (c) TEM image at 24 ^{o}C; (d) TEM image at 37 ^{o}C.

Previously, studies show that acetonitrile and methanol destabilize the zinc induced peptide nanotube formation. What's the mechanism on these phenomenons?

There're three possible models to explain the observed phenomena (Figure 2.22). In the first model, in the presence of solvent, peptide nanotubes dis-assemble to monomers, which subsequently self assemble into amyloid fibrils. Under this condition, the peptide arrangements in amyloid fibrils and nanotubes are different. In the second model, in the presence of solvent, instead of melting completely, peptide nanotubes decrease the sheet-sheet stacking and directly dis-assemble into amyloid fibrils. In this model, the nanotubes and fibrils share the same arrangement of peptides. The third model is the combination of the first two models. Peptide nanotubes can dis-assemble into not only fibrils but also monomers. Under these conditions, the amyloid fibrils could have two different kinds of peptide arrangements.

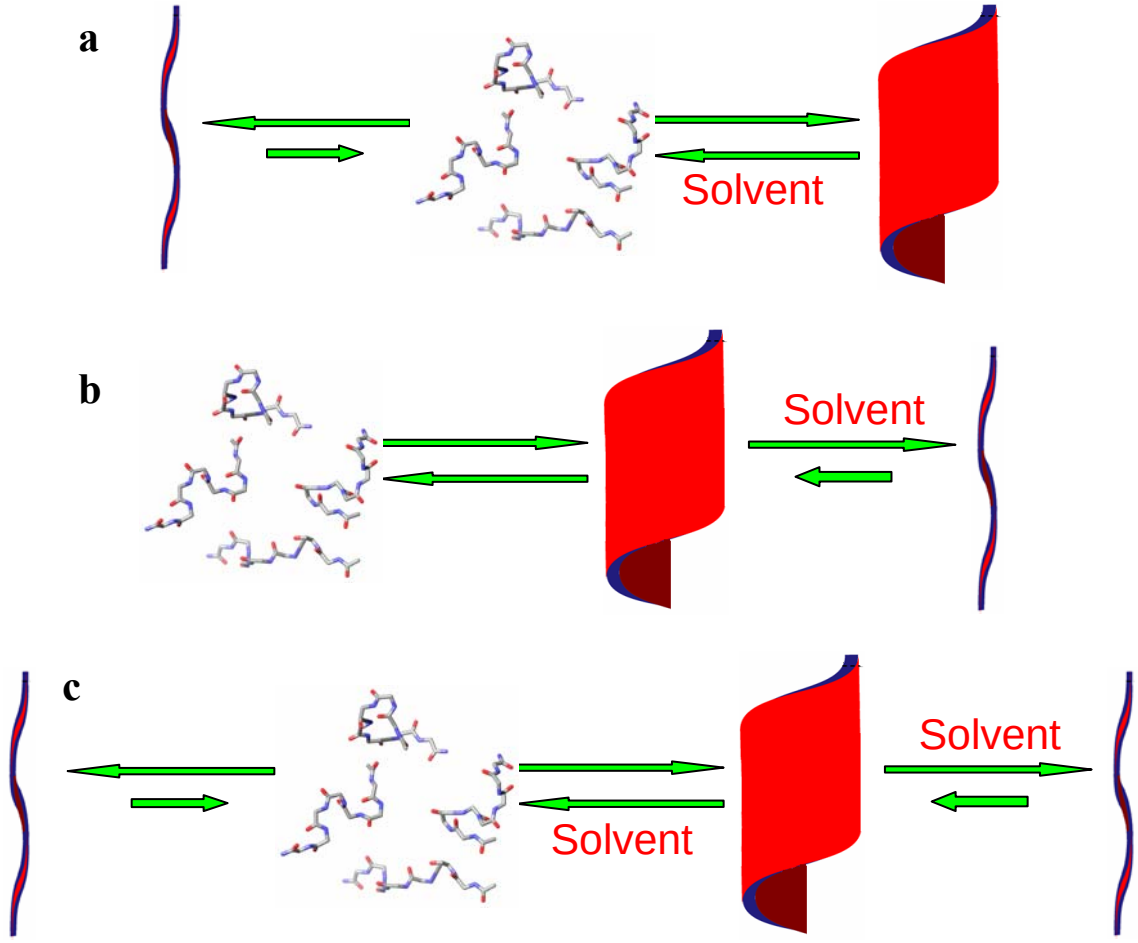

Figure 2.22. Three possible models for solvent effects. (a) In the presence of solvent, peptide nanotubes dis-assemble to monomers, which subsequently self assemble into amyloid fibrils; (b) in the presence of solvent, peptide nanotubes decrease the sheet-sheet stacking and directly dis-assemble into amyloid fibrils; (c) in the presence of solvent, peptide nanotubes can dis-assemble into not only fibrils but also monomers.

CONCLUSION

The self-assembly of Aβ(13-21)K16A shows different morphologies at different temperatures in the presence of zinc ions. In the presence of zinc ions, Aβ(13-21)K16A peptides self assemble into helical ribbons at low temperatures and nanotubes at high temperatures. Zn^{2+} induced ribbons can switch to Zn^{2+} induced nanotubes at elevated temperatures. Zn^{2+} induced peptide nanotubes are thermostable and do not break down at lower temperature.

ssNMR experiments were tried to clarify the detail peptide arrangement in zinc induced Aβ(13-21)K16A peptide nanotubes. Although several anions and ligands were tested, it is still difficult to bundle the peptide nanotubes.

Solvent effect on the zinc induced Aβ(13-21)K16A peptide self-assembly has been studied to learn the physical stability of peptide nanotubes. Some solvents, such as methanol and acetonitrile, can destabilize the peptide nanotubes. Zn^{2+} induced ribbons or nanotubes are more stable at lower temperature in the presence of acetonitrile.

CHAPTER 3

CONCLUSIONS AND PERSPECTIVES

The interaction and self-assembly of biomaterials, such as peptides, proteins, and lipids, are crucial to understanding of the principles underlying a variety of self-assembly associated conformational diseases, and to guide the development of materials for new opportunities in nanobiotechnology. Peptide self-assembly is mediated by weak, noncovalent bonds, such as hydrogen bonds, electrostatic interactions, hydrogen bonds, and van der Waals interactions. Although these bonds are relatively weak in isolation, as a combination, they govern the structural conformation of all biological macromolecules. On the other hand, peptide self-assembly and protein folding are also sensitive to outside environment, for example, temperature, pH, and ionic strength, which make the processes of protein folding and peptide self-assembly more complicated. Based on the understanding of the driving forces and mechanisms of peptide self-assembly, many novel self assembled supramolecular architectures have been fabricated.

In this dissertation, self-assembly of Aβ(13-21)K16A peptide originating from amyloid-β peptide was investigated *in vitro* and was specifically probed with zinc ions. Temperature effect of the self-assembly of this peptide was also investigated. In the presence of zinc ions, Aβ(13-21)K16A peptides self assemble into helical ribbons at low

temperatures, such as 4 ^{o}C and 24 ^{o}C. When increasing the temperature to 37 ^{o}C, these peptides self assemble into peptide nanotubes. Such nanotubes were also constructed with an even shorter peptide fragment of amyloid β peptide, Aβ(16-22), in the absent of metal ions (Lu 2003). Preformed helical ribbons can switch to peptide nanotubes with increasing temperature. Peptide nanotubes are quiet stable, and they cannot dissemble back to helical ribbons. The transition from helical ribbons to peptide nanotubes possibly results from the dramatic expansion of sheet-sheet lamination. The discovery of these peptide nanotubes is very important for novel material development.

ssNMR experiments were tried to clarify the detail peptide arrangement in zinc induced Aβ(13-21)K16A peptide nanotubes. Cryo- and lyo- experiments show that peptide nanotubes are destroyed during lyophilization. As a result, they need to be protected during the cryo- and lyo processes before the ssNMR experiments. Currently, the best method to protect peptide nanotubes from denaturation is to bundle the tubes. Several anions and chelates, such as SO_4^{2-}, EDTA, terephthalic acid, hydroquinone, 1,2-ethanedithion and 1,4-Benzenedimethanethiol, have been tested. However, these reagents cannot bundle the peptide nanotubes successfully. Future work needs to be focused on the protection of peptide nanotubes in the process of the preparation of ssNMR samples.

Solvent effects on the Zn^{2+} induced Aβ(13-21)K16A peptide self-assembly have been investigated to study the physical stability of peptide nanotubes. The results show that some solvents, such as methanol and acetonitrile, can destabilize the peptide nanotubes. The higher the solvent concentration, the less stable the peptide nanotubes. Temperature effect of the peptide self-assembly at certain solvent concentrations indicates that Zn^{2+} induced ribbons or nanotubes are more stable at lower temperature in

the presence of acetonitrile.

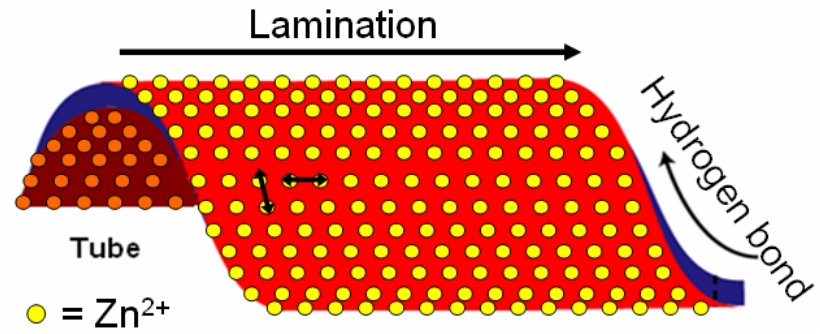

Figure 3.1. Zn^{2+} induced peptide nanotubes. Yellow dots represent zinc ions.

Future work needs to be focused on the exploring of nanotube functions. In Zn^{2+} induced peptide nanotubes, the zinc ion is partially proven to be coordinated to two histidines, one amine, and one water molecule. Zinc ions are also located on the surface of the peptide nanotubes in a repeating square pattern with 1 nm sides (Figure 3.1). Therefore, it is possible to design several substrates which coordinate to Zn^{2+} and are then located one by one on the surface of the peptide nanotubes with a 10 Å distance. If the reactive groups of two adjacent substrates, such as amino acids and short peptides, are close enough, peptide polymerization reactions can ensure. In this case, template is expanded from nucleic acids to prearranged zinc ions.

The next work is to explore the zinc-induced nanotubes for their novel catalytic chemistry. In Zn^{2+}-induced peptide nanotubes, zinc ions have tetrahedral coordination geometry, coordinating to two histidines, one amino group, and one water molecule, which is similar to zinc catalytic centers in most zinc enzymes. Therefore, the defined Zn^{2+} ions in Zn^{2+}-induced peptide nanotubes could very likely to serve as catalytic centers to mimic some zinc enzymes. As the binding ligands are at the N-terminal of the

amyloid peptide and located on the surface of the peptide nanotubes after self-assembly, it is possible to modify the binding ligands to generate the designed chemistry. Since zinc ions are packed on the surfaces of peptide nanotubes, highly packed zinc catalytic centers may significantly enhance reaction efficiency. These catalytic reactions also expanded the application of nano materials. The nano-scaled zinc induced peptide nanotubes can function not only as zinc enzymes, but also provide highly packed catalytic centers.

REFERENCES

Assaf, S. Y., Chung, S. H. **1984**. *Nature* 308: 734-6.

Benzinger, T. L., Gregory, D. M., Burkoth, T. S., Miller-Auer, H., Lynn, D. G., Botto, R. E., Meredith, S. C. **2000**. *Biochemistry* 39: 3491-9.

Burkoth, T. S., Benzinger, T. L. S., Urban, V., Morgan, D. M., Gregory, D. M., Thiyagarajan, P., Botto, R. E., Meredith, S. C., Lynn, D. G. **2000**. *J. Am. Chem. Soc.* 122: 7883-9.

Bush, A. I., Pettingell, W. H., Multhaup, G., Paradis, M. D., Vonsattel, J. P., Gusella, J. F., Beyreuther, K., Masters, C. L., Tanzi, R. E. **1994**. *Science* 265: 1464-7.

Carpino, L. A. and Han, G. Y. **1972**. *J Org Chem* 37: 3404-7.

Cherny, R. A., Atwood, C. S., Xilinas, M. E., Gray, D. N., Jones, W. D., McLean, C. A., Barnham, K. J., Volitakis, I., Fraser, F. W., Kim, Y., Huang, X., Goldstein, L. E., Moir, R. D., Lim, J. T., Beyreuther, K., Zheng, H., Tanzi, R. E., Masters, C. L., Bush, A. I. **2001**. *Neuron* 30: 665-76.

Curtain, C. C., Ali, F., Volitakis, I., Cherny, R. A., Norton, R. S., Beyreuther, K., Barrow, C. J., Masters, C. L., Bush, A. I., Barnham, K. J. **2001**. *J. Biol. Chem.* 276: 20466-73.

Dong, J., Shokes, J. E., Scott, R. A., Lynn, D. G. **2006**. *J. Am. Chem. Soc.* 128: 3540-2.

Fraser, P. E., Nguyen, J. T., Chin, D. T., Kirschner, D. A. **1992**. *J. Neurochem.* 59: 1531-40.

Ghadiri, M. R., Granja, J. R., Milligan, R. A., McRee, D. E., Khazanovich, N. **1993**. *Nature* 366: 324-7.

Hardy, J., Selkoe, D. J. **2002**. *Science* 297: 353-6.

Iijima, S. **2001**. *Nature* 354: 56-8.

Kirschner, D. A., Abraham, C., Selkoe, D. J. **1986**. *Proc. Natl. Acad. Sci. USA* 83: 503-7.

Liu, S. T., Howlett, G., Barrow, C. J. **1999**. *Biochemistry* 38: 9373-8.

Lu, K., Guo, L., Mehta, A. K., Childers, W. S., Dublin, S. N., Skanthakumar, S., Conticello, V. P., Thiyagarajan, P., Apkarian, R. P., Lynn, D. G. **2007**. *Chem. Com.* 2729-30.

Lu, K., Jacob, J., Thiyagarajan, P., Conticello, V. P., Lynn, D. G. **2003**. *J. Am. Chem. Soc.* 125: 6391-3.

Morgan, D. M., Dong, J., Jacob, J., Lu, K., Apkarian, R. P., Thiyagarajan, P., Lynn, D. G. **2002**. *J. Am. Chem. Soc.* 124: 12644-5.

Ozbas, B., Kretsinger, J., Rajagopal, K., Schneider, J. P., Pochan, D. J. **2004**. *Macromolecules* 37: 7331-7.

Pochan, D. J. Scheneider, J. P., Kretsinger, J., Ozbas, B., Rajagopal, K., Haines, L. **2003**. *J. Am. Chem. Soc.* 125: 11802-3.

Rapaport, H., Kjaer, K., Jensen, T. R., Leiserowitz, L., Tirrell, D. A. **2000**, *J. Am. Chem. Soc.* 122: 12523-9.

Ringler, P., Schulz, G. E. **2003**. *Science* 302: 106-9.

Sarikaya, M., Tamerler, C., Schwartz, D. T., Baneyx, F. **2004**. *Annu. Rev. Mater. Res.* 34: 373-408.

Schneider, J. P., Pochan, D. J., Ozbas, B., Rajagopal, K., Pakstis, L., Kretsinger, J. **2002**. *J. Am. Chem. Soc.* 124: 15030-7.

Scopes, R. K. **1994**. *Protein purification: principles and practice, 3rd edn.* Springer Verlag, New York.

Seeman, N. C., Belcher, A. M. **2002**. *Proc. Natl. Acad. Sci. USA* 99: 6451-55.

Sleytr, U. B., Schuster, B., Pum, D. **2003**. *IEEE Eng. Med. Biol. Mag.* 22: 140-50.

Southall, N. T., Dill, K. A., Haymet, A. D. J. **2002**. *J. Phys. Chem. B* 106: 521-33.

Sparks, D. L., Schreurs, B. G. **2003**. *Proc. Natl. Acad. Sci. USA* 100: 11065-9.

Studelska, D. R., McDowell, L. M., Adler, M., O'Connor, R. D., Mehta, A. K., Guilford, W. J., Dallas, J. L., Arnaiz, D., Light, D. R. and Schaefer, J. **2003**. *Biochemistry* 42: 7942-9.

Urry, D. W. **1993**. *Angew. Chem. Inr. Ed. Engl.* 32: 819-41.

Urry, D. W., Hugel, T., Seitz, M., Gaub, H. E., Sheiba, L., Dea, J., Xu, J., Parker, T. **2002**. *Phil. Trans. R. Soc. Lond. B* 357: 169-84.

Valèry, C., Paternostre, M., Robert, B., Gulik-Krzywicki, T., Narayanan, T., Dedieu, J., Keller, G., Torres, M., Cherif-Cheikh, R., Calvo, P., Artzner, F. P. **2003**. *Proc. Natl. Acad.*

Sci. USA 100: 10258-62.

Wang, W. **2000**. *Int. J. Pharm.* 203: 1-60.

Widom, B., Bhimalapuram, P., Koga, K. **2003**. *Phys. Chem. Chem. Phys.* 5: 3085-93.

Zhang, S. **2002**. *Biotech. Adv.* 20: 321-39.

Zhang, S. **2003**. *Nat. Biotechnol.* 21: 1171-8.